Filtenna Using Ultra-Wideband Fed Varactor Tuned Frequency Selective Surface

by

Jason Leo Durbin, B.S.E.E.

A Thesis

In

ELECTRICAL ENGINEERING

Submitted to the Graduate Faculty
of Texas Tech University in
Partial Fulfillment of
the Requirements for
the Degree of

MASTER OF SCIENCE

IN

ELECTRICAL ENGINEERING

Approved

Dr. Mohammad Saed
Chair of Committee

Dr. Changzhi Li

Peggy Gordon Miller
Dean of the Graduate School

August, 2011

ACKNOWLEDGEMENTS

First, I would like to thank my advisor, Dr. Mohammad Saed. Dr. Saed has helped develop me into the engineer I am today. I am thankful for all the opportunities he gave me throughout my undergraduate career in tutoring and undergraduate research. I'm glad we continued the professional relationship to my graduate studies – I don't think I could have picked a better advisor.

Thank you to my family. I can't imagine attempting to attain a higher degree without their support. My mother, Sandi, pushed me on even around finals when she would get the call from me saying, "Mom, I don't think I'm going to do very good this semester." I thank my father, Jeff, for the wisdom and common sense he passed down to me. Thanks to my sister, Shalane, for the support she gave. Especially for paying for the much needed vacations when things got tough. Lastly, thank you to my fiancée, Meredith. She may have come late in the game, but she helped pushed me on. I love you guys!

Thank you to Aeroflex/Metelics for the graciously donated varactors. Thanks for the speedy delivery varactors and the help in selecting the suitable varactor. Also, I'd like to thank the Roger's Corporation for the donated copper boards.

TABLE OF CONTENTS

ACKNOWLEDGEMENTS ii

ABSTRACT vi

LIST OF TABLES vii

LIST OF FIGURES viii

I. INTRODUCTION 1

1.1. Overview 1

1.2. Background 1

1.3. Chapter Summary 3

1.3.1. Chapter I: Introduction 3

1.3.2. Chapter II: Frequency Selective Surfaces 3

1.3.3. Chapter III: Ultra-Wideband Antenna 3

1.3.4. Chapter IV: Proposed Design 4

1.3.5. Chapter V: Conclusion and Suggested Improvements 4

II. FREQUENCY SELECTIVE SURFACES 5

2.1. Introduction 5

2.2. Design Considerations 6

2.3. FSS Characterization, Design, and Modeling 9

2.3.1. Fixed Frequency FSS 12

2.3.2. Tunable Frequency FSS 15

III. ULTRA-WIDEBAND ANTENNA 20

3.1. Introduction 20

3.2. Elliptical Monopole Antenna 22

3.2.1. Simple Monopole 22

3.2.2. Monopole with Ground Plane 24

3.2.3. Monopole with Aperture and Ground Plane 26

IV. PROPOSED DESIGN 29

4.1. Introduction 29

4.2. Individual Components 29

4.2.1. Frequency Selective Surface 29

4.2.2. Varactors 32

4.2.3. Elliptical Monopole Antenna 35

4.3. Simulated Results 35

4.3.1. Simple Design 35

4.3.2. Design with Bias Lines 41

4.3.3. Other Attempted Designs 44

4.4. Experimental Results 44

4.4.1. Tuning 45

4.4.2. Ground Distance 47

4.4.3. FSS Distance 49

4.4.4. Radiation 50

4.5. Discussion of Results 54

V. CONCLUSION AND SUGGESTED IMPROVEMENTS 56

5.1. Accomplishments 56

5.2. Suggested Improvements 56

5.2.1. Beam Steering 56

5.2.2. Increasing Tuning Range and Reducing Surface Wave Radiation 57

5.2.3. Improved Radiation 57

REFERENCES 58

A. VARACTOR APPROXIMATION 61

ABSTRACT

A varactor tuned frequency selective surface (FSS) is proposed. The FSS is a slotted ring design and is fed by an ultra-wideband (UWB) planar, elliptical, monopole antenna. The design produces a tuning range of 3.2 – 4.5 GHz over a varactor reverse bias voltage of 0 – 4.5 V.

In this paper, discussion of frequency selective surfaces – from design to modeling is proposed. Next, ultra-wideband antennas are discussed with emphasis on a planar, elliptical, monopole antenna. Simulations of the antenna and frequency selective surfaces are shown through Ansoft's HFSS. The proposed tunable structure is simulated using HFSS through two models – a simple model and a model with bias lines. The proposed structure is experimentally verified to prove the tuning ability. Finally, suggested improvements are proposed.

LIST OF TABLES

1. Dimensions for Parametric Characterizations 12
2. Frequency Selective Surface Parameters 30
3. Varactor Parameters [28] 33
4. Variable Definitions in Equation (1) [28] 33
5. Results from Las Vegas Varactor Curve Fitting 34
6. Parameters for Simulated UWB Fed, Tunable FSS 37

LIST OF FIGURES

1. Block Diagram Showing the Motivation of Employing FSS Structures [4] 2
2. Some Frequency Selective Surface Topologies [11] 7
3. Transparent and Reflective FSS Structures [11] 8
4. Reflection and Transmission Curves for Complementary Surfaces 9
5. Slot Ring FSS Unit Cell 10
6. Slot Ring Unit Cell FSS Model in HFSS 11
7. FSS Parameter Characterization Results in HFSS 13
8. Multi-Layer Response of FSS Structure 15
9. Capacitance of Varactor Versus Reverse Voltage [7] 16
10. Electric Field Distribution of Slotted Ring FSS 17
11. Capacitance Effects on Resonant Frequency of FSS 18
12. Varactor DC Bias Line Considerations 19
13. UWB Antenna Candidates [24] 20
14. Summarized Results of Elliptical Monopole Antenna in [23] 23
15. Radiation Patterns of the Elliptical Monopole Antenna in [23] 24
16. Elliptical Monopole with Ground Plane 25
17. Return Loss (dB) of Various Ground Distances (u_{Ground}) 26
18. Elliptical Monopole with Aperture and Ground Plane 27
19. Return Loss and Y-Z Radiation Pattern of Elliptical Monopole 28
20. Frequency Selective Surface Employed 30
21. Simulated Return Loss of FSS with Various Capacitance Values 31
22. Measured Varactor Capacitance versus Reverse Voltage [28] 32

23. Las Vegas Best Fit Curve for Varactor Capacitance versus Reverse Voltage 34

24. Diagram for Simple UWB Fed, Tunable FSS 36

25. Simulated Return Loss of Various Varactor Reverse Voltages 38

26. Return Loss and Y-Z Radiation Patterns at 4.675 GHz of Simple Structure Where Reverse Voltage is 2 V 39

27. Return Loss and Y-Z Radiation Patterns at 5.22 GHz of Simple Structure Where Reverse Voltage is 3 V 40

28. Bias Lines 41

29. Return Loss for Various Reverse Voltages with Bias Lines 42

30. Return Loss and Radiation at 4.9 GHz with a Reverse Voltage of 3 V 43

31. Prototype 45

32. Experimental Verification of Tuning 46

33. Demonstration of resonance splitting 47

34. Return Loss for Ground Distances of 10 mm and 15 mm 48

35. Return Loss for Ground Distances of 15 mm and 20 mm 49

36. Return Loss of Various Reverse Voltages where u_{FSS} = 5 mm; u_{Ground} = 20 mm 50

37. Radiation Patterns When Varactors are Biased at 2 V 51

38. Radiation Patterns When Varactors are Biased at 3 V 52

39. Radiation Patterns When Varactors are Biased at 2 V with Ground 53

40. Radiation Patterns When Varactors are Biased at 3 V with Ground 54

41. Measured and Simulated Results at 2 V Reverse Voltage 55

CHAPTER I

INTRODUCTION

1.1. Overview

The purpose of this thesis is to explore the filtering characteristics of a frequency selective surface (FSS) to be used with an ultra-wideband (UWB) antenna. The structure is tuned using a varactor, or a voltage-controlled capacitor. The antenna is a simple elliptical monopole antenna with UWB characteristics. This paper explores the feasibility of tuning the UWB antenna to reduce the necessity of a bandpass filter after the antenna.

Investigations into FSS structures and UWB antennas are shown in this paper. Varactor and varactor biasing considerations are discussed. The structure is simulated by Ansoft's HFSS and is experimentally verified to produce tuning characteristics.

1.2. Background

Filtering antennas, or "filtennas," perform filtering operations on antennas. Filtennas are employed in receiver front ends to relieve the necessity of filters following the antenna. Filtennas with notch-band performances are extremely popular with UWB antennas to remove the IEEE 802.11a wireless local area network (WLAN). [1] proposes an UWB antenna with slots that provide notching characteristics in the WLAN band (5.12 – 5.85 GHz). The notching characteristics of the filtennas are usually produced by modifying the antenna itself. Reference [2] proposes placing a bandpass filter (BPF) and notching filter before the antenna, without actually modifying the antenna. However, this

is identical to placing a filter after an antenna; the design is just planar instead of discrete elements.

Investigations of the filtering aspects of the FSS placed on the antenna serve as the primary concern for this research. The authors of [3] propose placing a band-pass FSS in the aperture of a horn antenna to narrow the bandwidth of the antenna. Reference [4] proposes a miniaturized FSS on a patch antenna array to create a more narrow response from the patch antenna. Figure 1 demonstrates the motivation of the FSS implementation in [3]. The FSS and antenna act as filtenna, and as mentioned previously, the filtenna relieves the necessity of the BPF in the receiver. The two papers, [3] and [4], demonstrate a fixed frequency filtering structure from the FSS. Other applications of placing an FSS near an antenna is to improve the antenna's directivity and radiation efficiency [5], [6]. Also, [7] investigates a multi-layer FSS structure to produce a beam steering application.

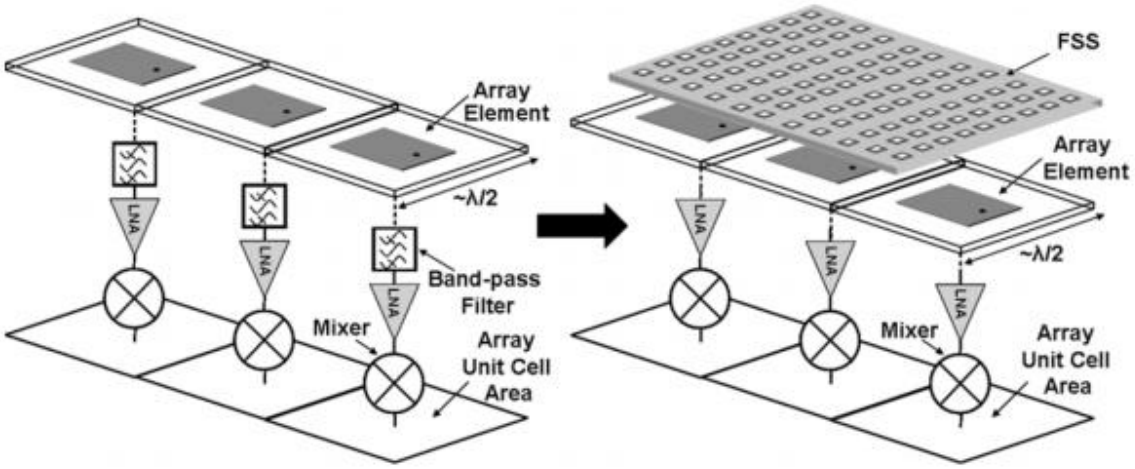

Figure 1: Block Diagram Showing the Motivation of Employing FSS Structures [4]

The thesis in [8] discusses the tuning aspects of the miniaturized FSS shown in [4]. The authors of [7] propose a tunable band-pass FSS with insight into varactor considerations. However, as mentioned previously, [7] demonstrates the tunability for beam steering applications with each row of varactors being able to be tuned independently. Other varactor tuned frequency selective surfaces are discussed and investigated in [9], [10].

1.3. Chapter Summary

1.3.1. Chapter I: Introduction

Chapter I introduces the reader to filtennas and shows the motivation for the tunable FSS and UWB structure. Insight into filtennas is given. Also, investigations into placing FSS structures in the near-field of an antenna are discussed..

1.3.2. Chapter II: Frequency Selective Surfaces

Frequency selective surfaces pose an important role in the overall design of the structure proposed in this research. Chapter II discusses different topologies available and the research done these topologies. The filtering response is shown. Also, considerations on creating a tunable FSS are demonstrated. Simulation results are presented for multi-layer FSS, fixed frequency FSS, and varactor tuned FSS structures.

1.3.3. Chapter III: Ultra-Wideband Antenna

Considerations in deciding the UWB antenna suitable for this research are discussed in Chapter III. Return loss and radiation patterns are considered for each proposed design.

1.3.4. Chapter IV: Proposed Design

The final design is shown in Chapter IV. The simulated results of a simple design without bias lines are discussed first. Next, the simulation results of the design with bias lines are demonstrated. The experimental results that demonstrate the tuning of the structure are shown. Return loss and radiation patterns are considered in the chapter. Lastly, a comparison of simulated and experimental results is shown.

1.3.5. Chapter V: Conclusion and Suggested Improvements

Finally, Chapter V concludes the thesis with conclusions and proposed improvements.

CHAPTER II

FREQUENCY SELECTIVE SURFACES

2.1. Introduction

Frequency selective surfaces (FSS) have been extensively researched and explored for many years. FSS structures are generally periodically arranged. The FSS frequency characteristics depend solely on the dimensions of the elements and substrate properties. FSS applications vary almost as much as their structures and designs. Radomes were the first application to employ FSS structures [11]. These radomes, "hybrid radomes," use FSS structures to make the radome appear transparent to the antenna at the operating frequency. Other applications exist such as spatial filters, reflectors, and absorbers for electromagnetic interference (EMI) [11].

Frequency selective surfaces can operate as bandstop or bandpass filters depending on the design. Much research in FSSs has been biased towards optimizing the structures for stopband performance. The emphasis on stopband performance has a significant use in the industry, such as notching the IEEE 802.11a frequency band [1] in ultra-wideband (UWB) applications. The miniaturized FSS demonstrated in [12] explores the structures as bandpass structures. This thesis investigates a bandpass type of FSS topology.

Originally, geometry modifications of the FSS structure demonstrated frequency selectivity variations. As proposed in [13], stub-loading a FSS can give rise to resonant frequency shifts and bandwidth reduction. Then, [14] demonstrated discrete element

reactive loading of FSSs to demonstrate frequency tunability feasibility (discrete frequency). The idea of adding discrete elements then gave rise to adding varactors to FSS structures to create the ability to electronically tune the resonant frequency [9]. Other methods of FSS tunability have been proposed, such as microelectromechanical (MEMS) designs [15] - [16]. Some have demonstrated FSS tunability by modifying the substrate characteristics by adding liquid metal slugs in [17] and a liquid filled substrate in [18].

This chapter begins by discussing design considerations of frequency selective surfaces. Bandpass and bandstop FSS structures are shown. Computer modeling of frequency selective surfaces through Ansoft's HFSS™ is demonstrated. Next, the FSS employed by this project will be characterized. Lastly, tuning of the FSS structure implementing a varactor will be demonstrated through simulations.

2.2. Design Considerations

Various topologies exist for frequency selective surfaces. The shape of FSSs depend highly on the design specifications. Each layout of equivalent size may have varying resonant frequencies. Some structures may create a multi-band operation [19], while most will be single resonant (excluding spurious bands). The polarization and angle of incidence are also important considerations. Not all FSS structures resonate at all angles of incidence [11]. Angle of incidence may change the resonance and bandwidth of the FSS [20]. However, angle of incidence and polarization is not discussed in this thesis because the structure is placed in the near-field of an antenna. Figure 2 shows some common FSS topologies [11]. The structures are divided into four groups as given by [11].

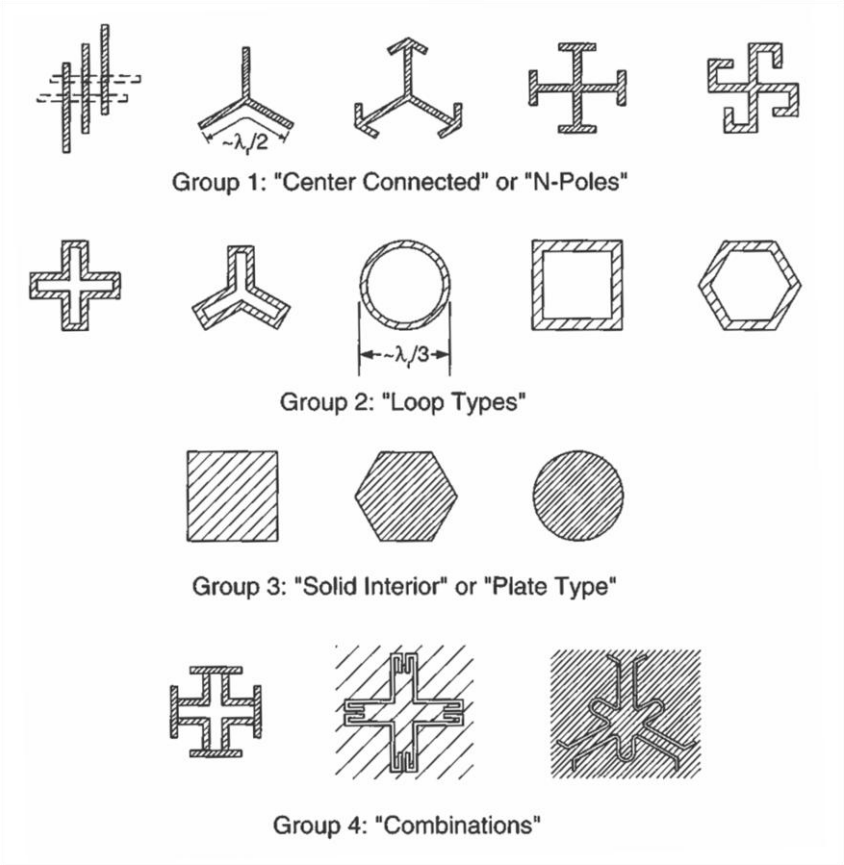

Figure 2: Some Frequency Selective Surface Topologies [11]

Frequency selective surfaces are also divided into two categories: transparent and reflective. These two surfaces are said to be complementary of each other. Reflective surfaces reflect the frequency of interest while appearing transparent to all other frequencies. Reflective surfaces act as bandstop filters. Conversely, transparent surfaces appear transparent at the frequency of interest, while reflecting all other undesired frequency. Transparent surfaces create a bandpass performance and are the primary surface type discussed in this paper. Figure 3 shows the topological differences between transparent and reflective surfaces [11]. Babinet's Principle states that complementary surfaces (transparent and reflective) of the same dimensions must have identical resonant

frequencies [11]. However, for Babinet's Principle to be valid a few caveats must be observed: the metal must be thin (~1/1000λ), thicker substrates produce non-symmetrical results, and cascading surfaces to produce a multiple layer structure causes differing results [20]. Figure 4 demonstrates Babinet's Principle on a complementary circular loop pair. As can be seen in the figure, the transmission of the transparent surface is almost identical to the reflection of the reflective surface (and vice-versa).

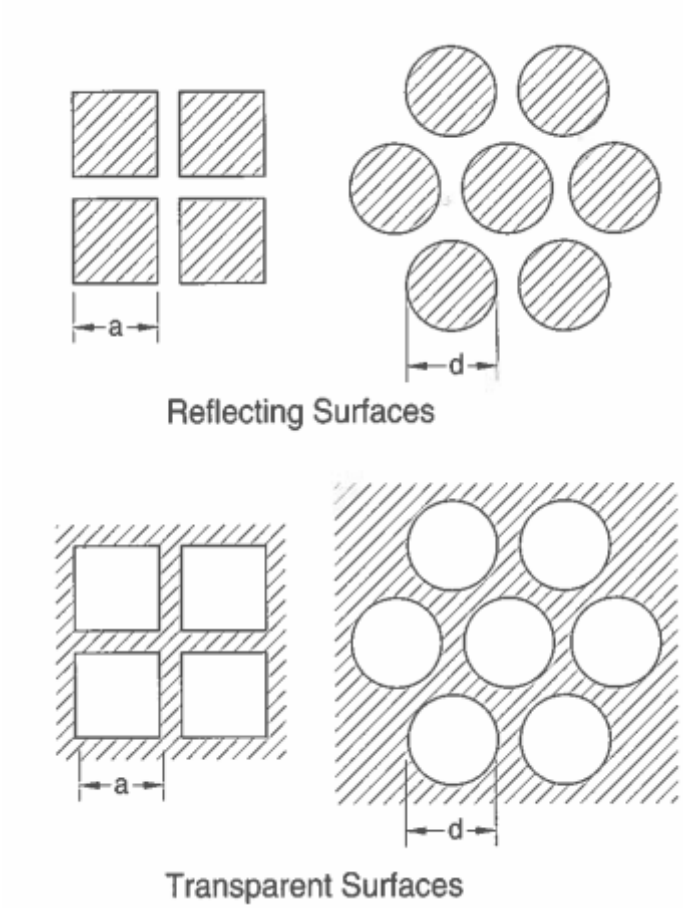

Figure 3: Transparent and Reflective FSS Structures [11]

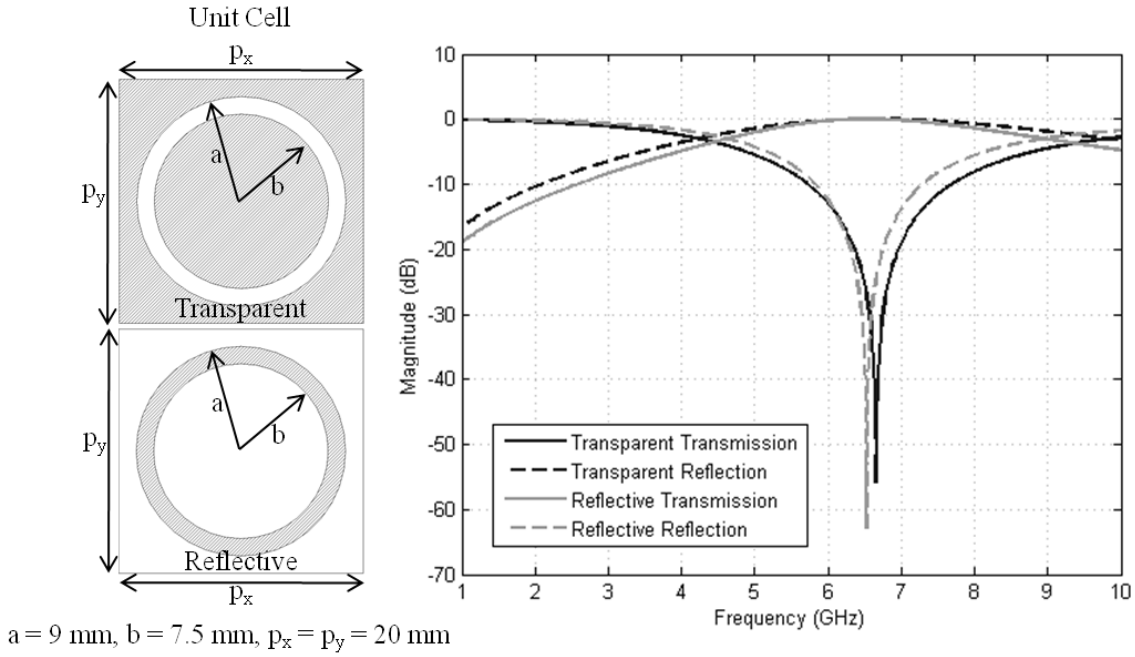

Figure 4: Reflection and Transmission Curves for Complementary Surfaces
Surfaces are simulated in air.

This thesis is primarily concerned with transparent surfaces because a bandpass response is desired. The FSS configuration must pass desired frequency, while reflecting all unwanted frequencies back to the antenna (bandpass – transparent surface). Also, the FSS element used in this research is a circular ring slot (Figure 2, Group 2). The ring slot is chosen to provide a convenient method for biasing, as will be discussed with the inclusion of the varactor for tuning (Chapter IV section 4.3.2).

2.3. FSS Characterization, Design, and Modeling

Design equations for frequency selective surface seem to not exist. As discussed in [20], the development of FSS structures begins with a simple dipole surface. The topology then proceeds to loaded dipoles and ring types. Many of the FSS topologies

discussed in [11] show the reflection or transmission of a given FSS, but not much discussion in the design. This section will characterize the selected FSS structure for this project. As mentioned previously, the FSS design is a bandpass (transparent) loop design. An alternate and more common description of the FSS is a "slotted ring." Figure 5 shows the shape and parameters of the FSS available for optimization.

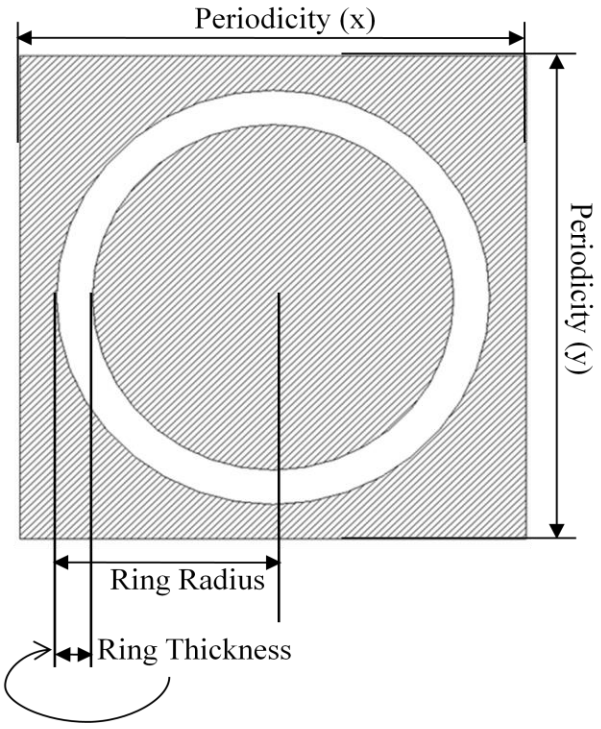

Figure 5: Slot Ring FSS Unit Cell

HFSS™, Ansoft's 3D electromagnetic full-wave solver, is selected to simulate the FSS structures. To simulate an infinite, periodic, FSS structures, the FSS must be surrounded by a box with sides of symmetry planes [21]. Figure 6 shows the unit cell model of an FSS in HFSS. Notice the perfect electric conductor ("E") and perfect magnetic plane ("H"), labeled (a) and (b) respectively. The perfect "E" is indicated by the

line-filled rhomboid; the perfect "H" is shown with no fill. Orientation of the electric and magnetic walls is important when placing the varactor (discussed in section 2.3.2). The remaining two planes of the rectangular prism are wave-ports, labeled (c) and indicated by a solid grey rhomboid. Cartesian coordinate axes are shown for both the 2-D and 3-D view to show orientation. The varactor is simulated using a "lumped RLC" boundary with a variable capacitance value. The substrate is shown beneath the FSS.

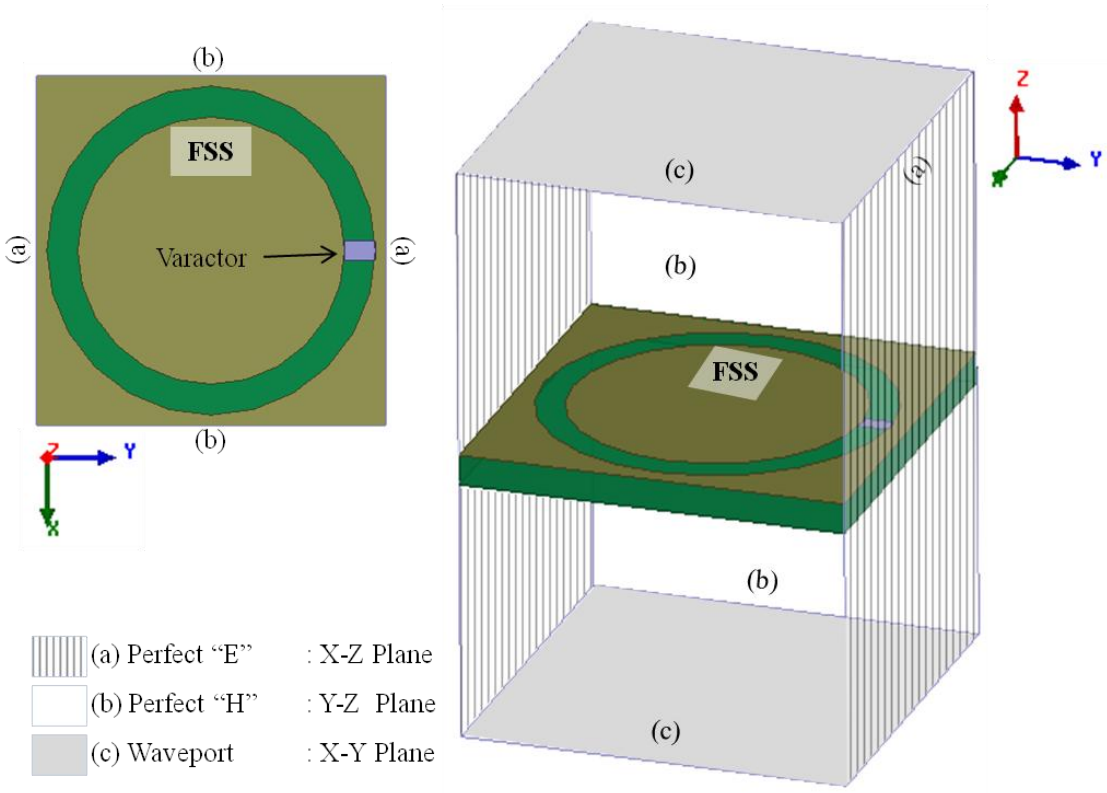

Figure 6: Slot Ring Unit Cell FSS Model in HFSS
2-D (top left), 3-D (right), and plane legend (bottom left). Axes indicate orientation.

Fixed frequency parameter characterization (ring radius, ring thickness, periodicity) of the slotted ring (Figure 5) using HFSS is discussed in Section 2.3.1.

Section 2.3.1 will also discuss cascading multiple layers of the bandpass structures. Varactor tuning (using HFSS) and bias line considerations are discussed section 2.3.2.

2.3.1. Fixed Frequency FSS

Using the method discussing previously, HFSS™ is able to effectively characterize the frequency selective surface. Table 1 shows the parameters used to characterize the FSS topology for the three parametric sweeps. Figure 5 may be used as a reference to indicate how the parameters relate to the given FSS structure. If the sweep indicates no substrate is used, the FSS structure is suspended in air. Otherwise, Roger's Duroid 5870 ($\varepsilon_r = 2.33$) is used as the substrate. The substrate thickness is 62 mils.

Table 1. Dimensions for Parametric Characterizations

Parameter Under Test	**Ring Radius (mm)**	**Ring Thickness (mm)**	**Periodicity**	**Substrate Thickness (mil)**	**Substrate Permittivity (ε_r)**
Periodicity	9	1.5	*UT*	62	2.33
Radius	*UT*	1.5	$2R^{\dagger}$ + 2mm	62	2.33
Ring Thickness	9	*UT*	20mm	62	2.33

† Where R is the ring radius. *UT* signifies that parameter is under test.

The resonant frequency of the FSS is estimated by finding the frequency where the minimum reflection (S_{11}) occurs. Figure 7 shows resonant frequency of the FSS versus the various parameters. As expected and as shown in the figure (top left), the ring radius most drastically changes the resonant frequency of the surface. Following shows the relationships inferred from the figures, where f_0 is the resonant frequency. The

relationships are based on crude curve fitting; the proportionality constants are neglected in the summary.

$$f_0 \propto t; \qquad \mathrm{t} = \text{Ring Thickness}$$

$$f_0 \propto \frac{1}{R^{1.25}}; \ \mathrm{R} = \text{Ring Radius}$$

$$f_0 \propto P^{.15}; \quad \mathrm{P} = \text{Periodicity}$$

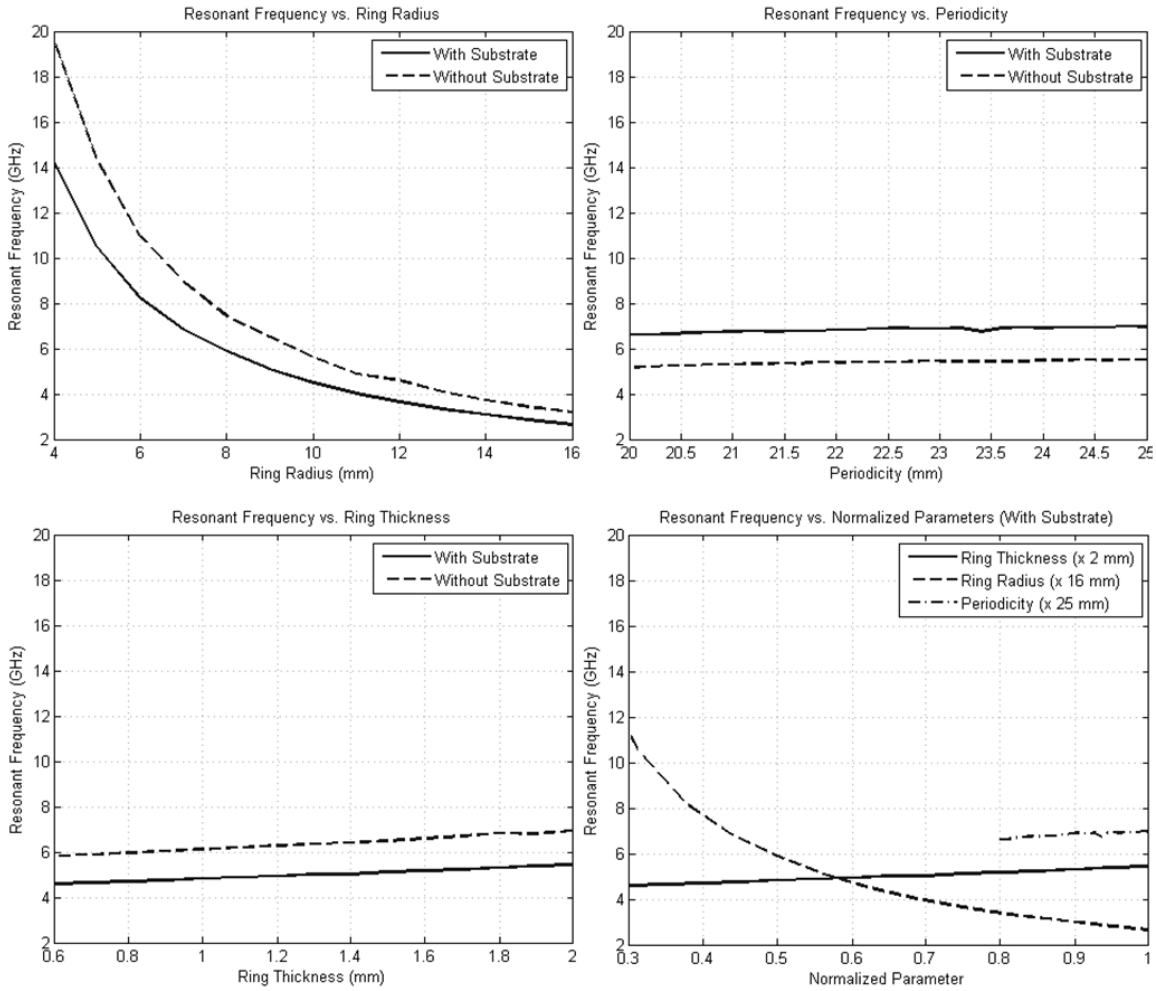

Figure 7. FSS Parameter Characterization Results in HFSS
Resonant frequency vs.: ring radius (top left), periodicity (top right), ring thickness (bottom left). Bottom right shows the resonant frequency vs. normalized parameters on the same plot for comparison (with substrate). Refer to Figure 5 and Table 1 for parameter declarations.

The periodicity and ring thickness have small but noticeable effects on the resonant frequency. Also, as mentioned in [8] and [11], the periodicity will affect grating lobes; with larger periodicity producing earlier grating lobes. Smaller periodicity is usually preferred [8]. The antenna and FSS structure in this paper is focused on adjusting the periodicity of the FSS to allow better coupling between the antenna and FSS rather than adjusting the periodicity to reduce grating lobes (Chapter IV). Also, a smaller periodicity produces a larger bandwidth of the FSS [11]. Because, varactor tuning will modify the bandwidth by adding additional capacitance; bandwidth effects are also neglected.

Finally, by adding layers, a bandpass (or bandstop) filter with a sharper cut-off can be synthesized. Figure 8 shows the frequency response of a multi-layer FSS (1-7 layers). The layers are all equally spaced at 11.72 mm. The ring radius is 9 mm, periodicity is 20 mm, the ring thickness is 1.5 mm, and the substrate is absent. Reference [11] states that cascading multiple layers with no dielectric "has considerable bandwidth variation as a function of angle of incidence." However, as mentioned previously, angle of incidence is not a concern in this paper because the FSS will be in the near-field of an antenna and the effects of the angle of incidence are different than normally investigated (FSS in antenna far-field). The layer spacing may be tuned to synthesize a better response in the pass-band if desired.

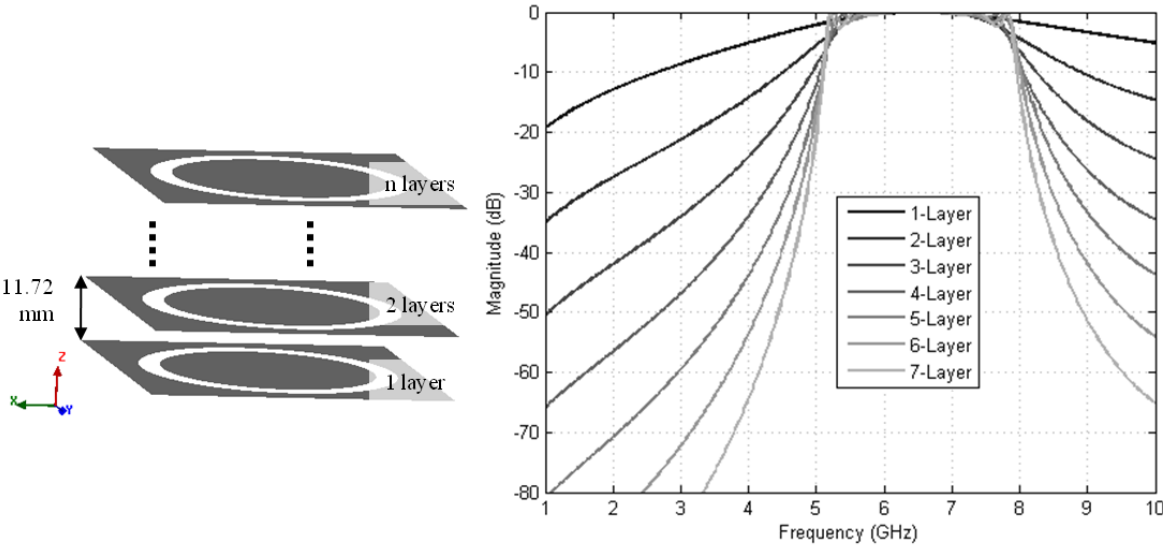

Figure 8: Multi-Layer Response of FSS Structure
No substrate. Layers equally spaced by 11.72 mm, ring radius is 9 mm, ring thickness is 1.5 mm and periodicity (x and y) is 20 mm.

2.3.2. Tunable Frequency FSS

As demonstrated in [14], adding reactive elements to the FSS designs modifies the bandwidth and resonant frequency characteristics. The concept in [14] demonstrates the resonant frequency shifts when adding discrete capacitors and inductors. The tunability is further explored in [10], [22], [9], and [12] by adding varactors instead of capacitors. A varactor is a special reversed biased diode that changes capacitance based on the DC voltage. Figure 9 shows an example of the capacitance of a varactor versus reverse biased DC voltage [7]. By controlling the bias voltage of the varactor, thus controlling the capacitance, the resonant frequency of the frequency selective surface can be tuned.

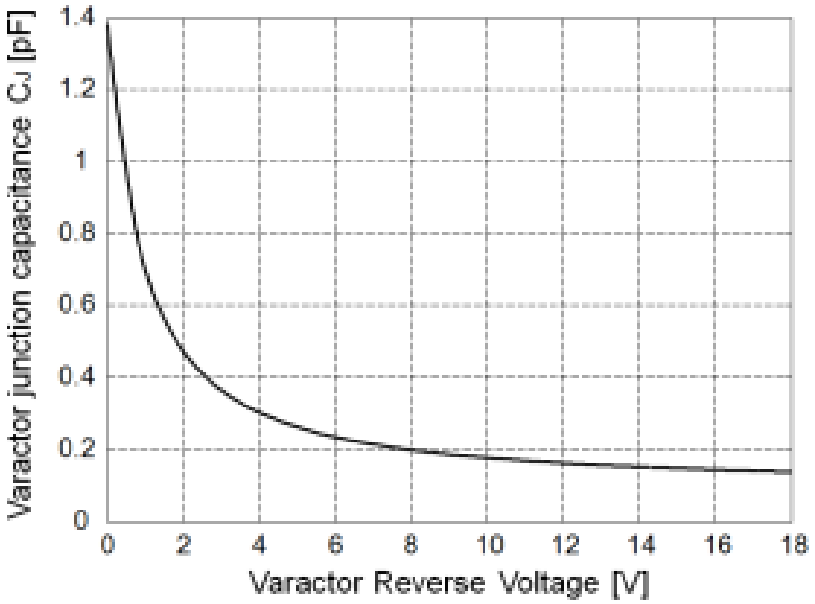

Figure 9. Capacitance of Varactor Versus Reverse Voltage [7]

Using Ansoft's HFSS™ and the method mentioned previously, the effect of the capacitance (simulating the varactors) on the resonant frequency of FSS can be demonstrated. Placement of the capacitor (or varactor) is crucial to the success of the tuning. The capacitor must be placed where a maximum occurs in the electric field distribution. As shown by Figure 10, the electric field maximum occurs along the Y-axis (for the given slotted ring), signifying the capacitor must lie parallel to the Y-axis. Placing the capacitor in the X-axis will result in frequency tuning; however, the tuning range of the FSS will be very limited compared to capacitance orientated in the Y-direction.

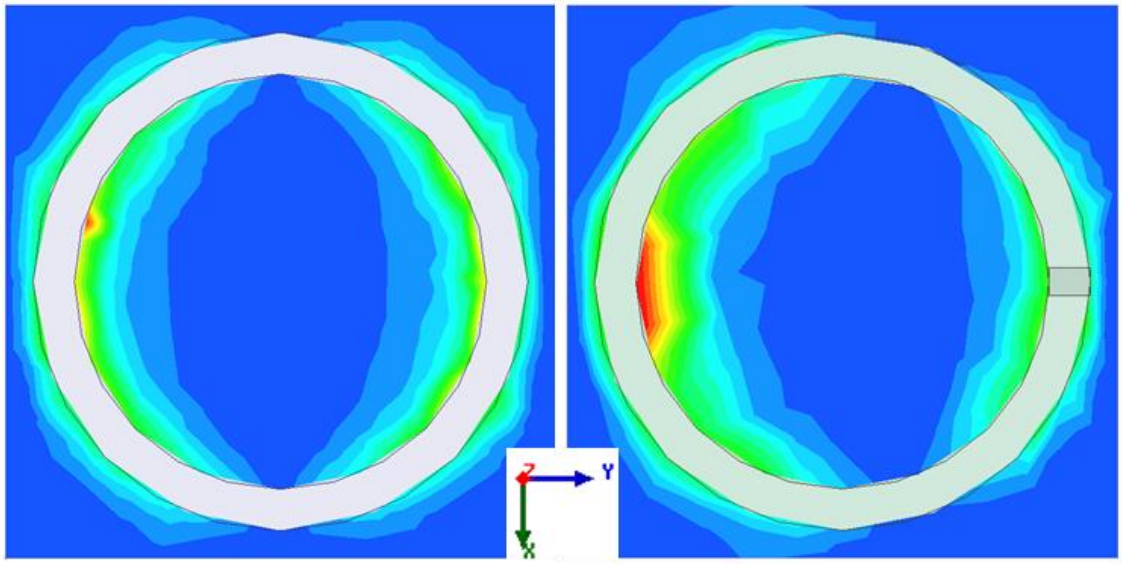

Figure 10. Electric Field Distribution of Slotted Ring FSS
Without capacitor (left) and with capacitor (right). Capacitor is indicated by a rectangle. Substrate thickness = 62 mils, ε_r = 2.33, ring radius = 9 mm, ring thickness = 1.5 mm, and periodicity = 20 mm, capacitance = 0.3 pF.

Figure 11 shows the return loss of the slotted ring surface with various capacitance values (top). As can be seen from the figure, as the capacitance increases the resonance decreases. This result agrees with [22], [9], and [12]. Figure 11 also shows the relationship of resonant frequency versus capacitance (bottom). In this simulation the ring radius is 9 mm, ring thickness is 1.5 mm, periodicity is 20 mm, and the substrate thickness is 62 mil with ε_r = 2.33. The capacitance orientation is also consistent with Figure 10. With a capacitance range from 0.1 – 1.3 pF and the given parameters, the FSS can achieve a tuning range of 2.9 – 4.6 GHz. The capacitance value changes the bandwidth and therefore reaffirms the reasoning of why the periodicity affects on bandwidth are neglected (mentioned in section 2.3.1).

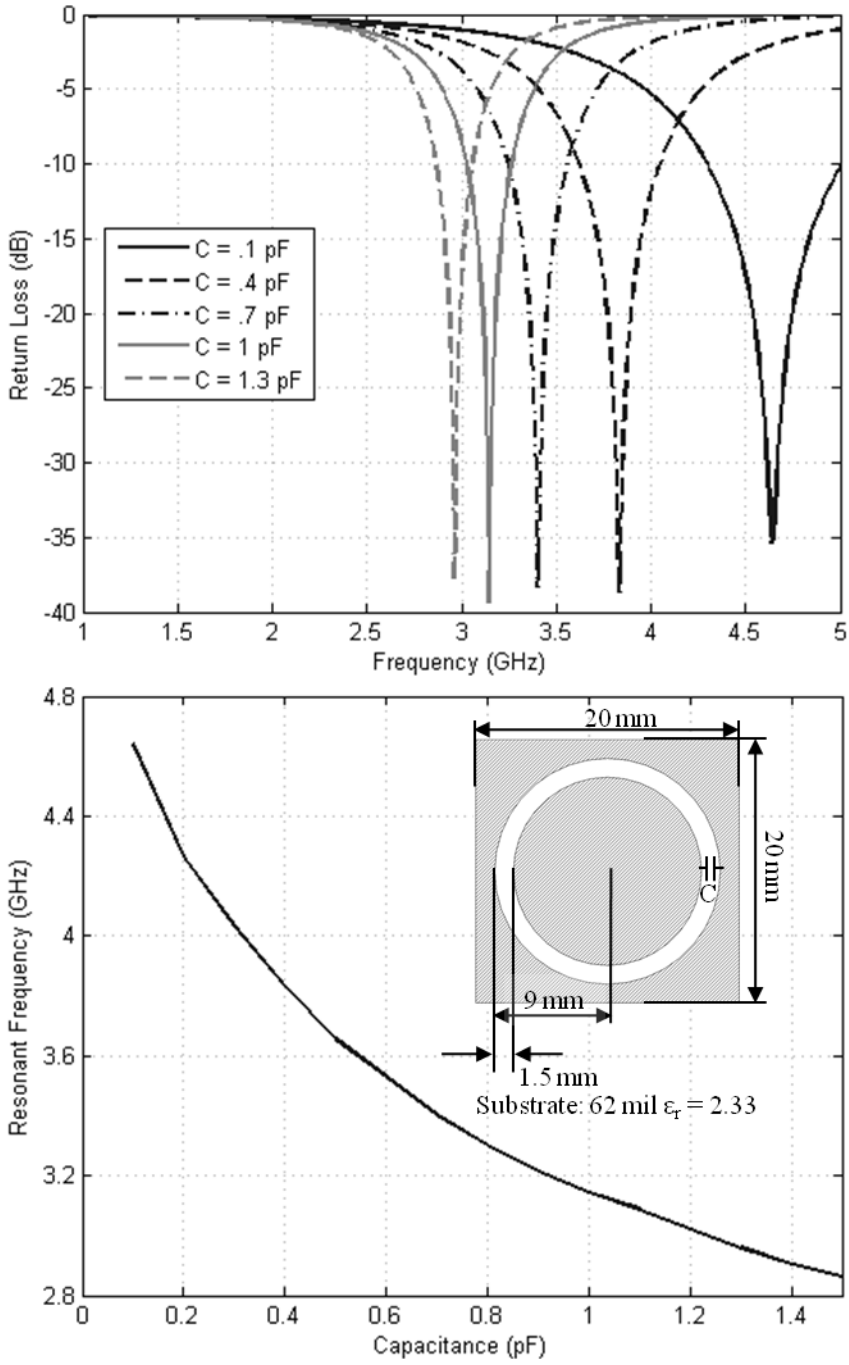

Figure 11. Capacitance Effects on Resonant Frequency of FSS
Return Loss of FSS with various capacitance values (top), resonant frequency of FSS vs. capacitance (bottom), and FSS dimensions with capacitance orientation inset on bottom figure.

The capacitance values in the simulations are relatively small (~ 0.3 pF). To provide a larger capacitance within the desired frequency range, the ring radius must shrink. However, making the capacitance value too large will cause the FSS to resonate no longer. This conclusion places special consideration on the capacitance value of the varactors that will be employed in the final design.

Lastly, special care must be used when deciding on a varactor controlled FSS because of the DC bias lines. The slotted ring design was chosen because the inner ring may be used to connect to one terminal of the DC source with the other terminal connected to the outer conductor. Figure 12 shows the placement of the varactor and bias line for this proposed design (left). The addition of the vias is discussed in Chapter IV section 4.3.2, where it is shown that the vias actually positively affects the overall structure of the antenna and FSS. Other methods of biasing place small slots in the FSS plane to provide isolation between the DC and ground [7]. The slots must be very small (< 0.2 mm) to not negatively affect the FSS design by adding parasitic reactance. Figure 12 also shows the biasing method demonstrated by [7] (right).

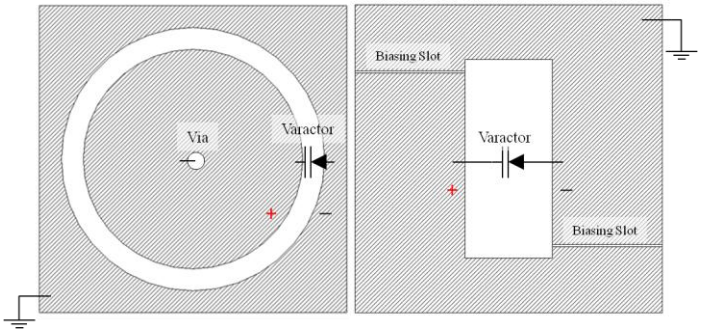

Figure 12. Varactor DC Bias Line Considerations
Proposed biasing scheme (left) and biasing scheme by [7] (right). Notice the biasing slots employed by [7] (width of 0.2 mm)

CHAPTER III

ULTRA-WIDEBAND ANTENNA

3.1. Introduction

Ultra-wideband (UWB) is defined by the Federal Communications Commission (FCC) as 3.1 to 10.6 GHz, and has attracted much attention since the band was allocated in 2002 [23]. UWB antennas are desired in this project so that the antenna will not be the limiting factor in tunability of the structure. Also, this thesis may serve as a basis for creating a tunable structure that can cover the entire UWB frequency range. Figure 13 shows images of three common UWB antennas discussed in [24] (Vivaldi, sinuous antenna, and a planar monopole).

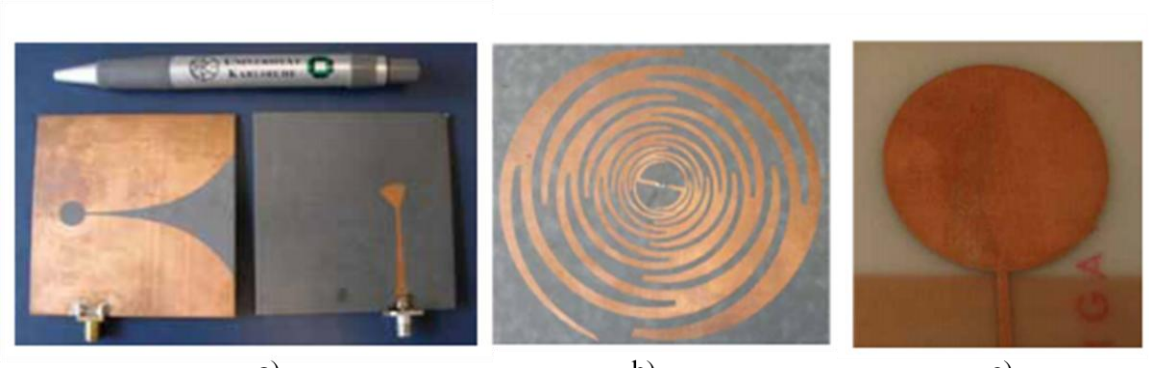

a) b) c)

Figure 13. UWB Antenna Candidates [24]
a) Vivaldi antenna, b) Sinuous antenna, c) Planar monopole

While many UWB antenna topologies exist, not all serve as a suitable solution for this project. The desired characteristics of the UWB antenna are: broadside radiation, planar topology, and simple structure. Broadside radiation, as opposed to end-fire

radiation, is desired so the FSS may lay parallel to the topology and reduce the overall size of the structure. A planar topology is desired (microstrip or coplanar waveguide), again, to reduce the size. Finally simplicity is desired so design time of the antenna may be minimized and a larger portion of time may be devoted to optimizing the final project.

Vivaldi antennas (Figure 13 a.), probably the most common UWB antenna of recent times, produce desirable bandwidth; however the Vivaldi radiation is end-fire, thus not fulfilling the first requirement of the antenna. Frequency independent spiral antennas (Figure 13 b.) provide suitable bandwidth and radiation patterns; however, spiral antennas are complex in design. Planar monopole antennas (Figure 13 c.), finally, provide a suitable solution as an antenna.

A simple coplanar waveguide (CPW) fed elliptical monopole antenna is proposed and investigated in [25]. This is further extended in [23] by a microstrip fed monopole antenna and serves as the basis for the UWB antenna employed in this research. Further investigation into improving the bandwidth by modifying the structure is shown in [26]. [23] and [26] extend the results by discussing resonant modes of the monopole antennas. Finally, [27] demonstrates a slot antenna with a U-shaped tuning stubs. Though, the antenna is a slotted kind, the results show an impedance bandwidth of a microstrip fed U with a reflector to be 2-9 GHz. [27]. So, [27] led to an investigation of adding an aperture to increase the bandwidth with the addition of a reflector.

3.2. Elliptical Monopole Antenna

An elliptical monopole antenna provides a suitable solution for the FSS feed because monopole antennas are simple, broadside radiation, and planar. This section discusses the planar elliptical monopole antenna proposed in [23]. The antenna results are summarized and discussed in section 3.2.1. The addition of a reflector behind the monopole is proposed in section 3.2.2. Finally, a brief discussion of adding an aperture to in increase the bandwidth with the reflector is discussed in section 3.2.3.

3.2.1. Simple Monopole

A simple, planar, microstrip fed, elliptical monopole antenna is investigated in [23]. The planar, elliptical monopole is desired because the design is simple and small. Figure 14 shows the summarized results of the research [23]. The figure shows the antenna is fed with a microstrip line on the smaller side of the ellipse. The investigation further builds on [25], which focused on a coplanar waveguide (CPW) fed elliptical monopole antenna. Reference [23] also shows a resonant mode analysis of the elliptical monopole antenna.

A further discussion of the effect of the "Gap" (Figure 14) and axial ratio (A/B) is discussed in [23], with the optimized parameters shown in Figure 14. As shown in Figure 14, the elliptical monopole antenna produces a significant bandwidth (3-12 GHz). This large bandwidth is desired for this project so the FSS may be the limiting factor in tunability, not the antenna.

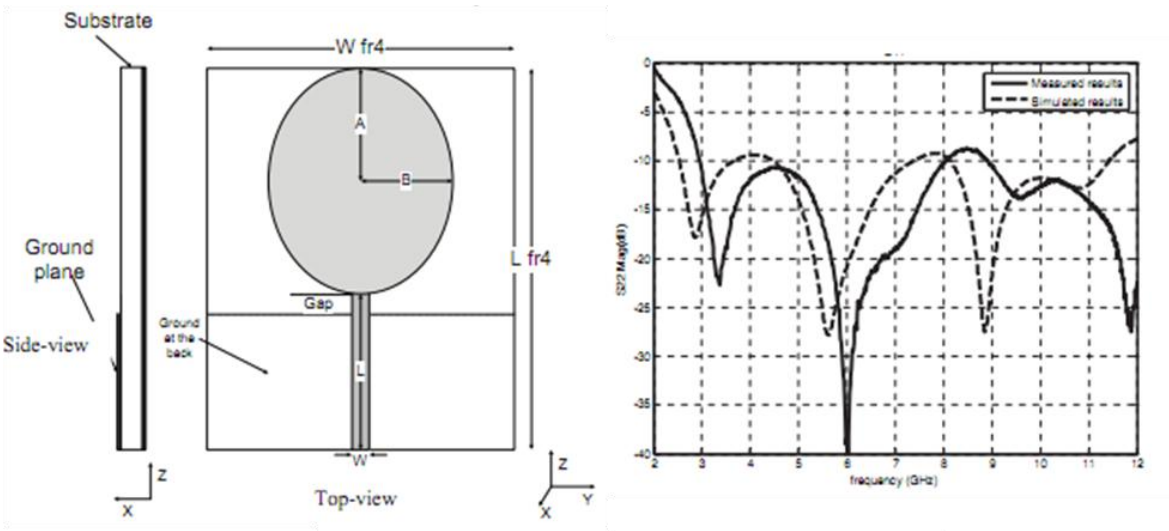

Antenna Parameters	Values
Length of ground (L_{ground})	*15mm*
Width of ground(W_{ground})	*36mm*
Major radius of ellipse (A)	*12mm*
Minor radius of ellipse (B)	*8.5mm*
Dimension between pole and ground (Gap)	*1mm*

Figure 14. Summarized Results of Elliptical Monopole Antenna in [23]

Radiation pattern of the monopole is important. A broadside radiation pattern is desired so the final structure size may be reduced. End-fire radiation requires the antenna be placed perpendicular to the FSS, and producing a larger final design. Figure 15 shows the radiation pattern of various frequencies of the elliptical monopole antenna [23]. The monopole demonstrates almost isotropic radiation in the X-Y plane. The radiation pattern demonstrates the desired broadside radiation. However, the radiation from the back is undesired because only on FSS structure will be employed on one side to filter the antenna. To reduce the back radiation the addition of a ground plane is invested in section 3.2.2.

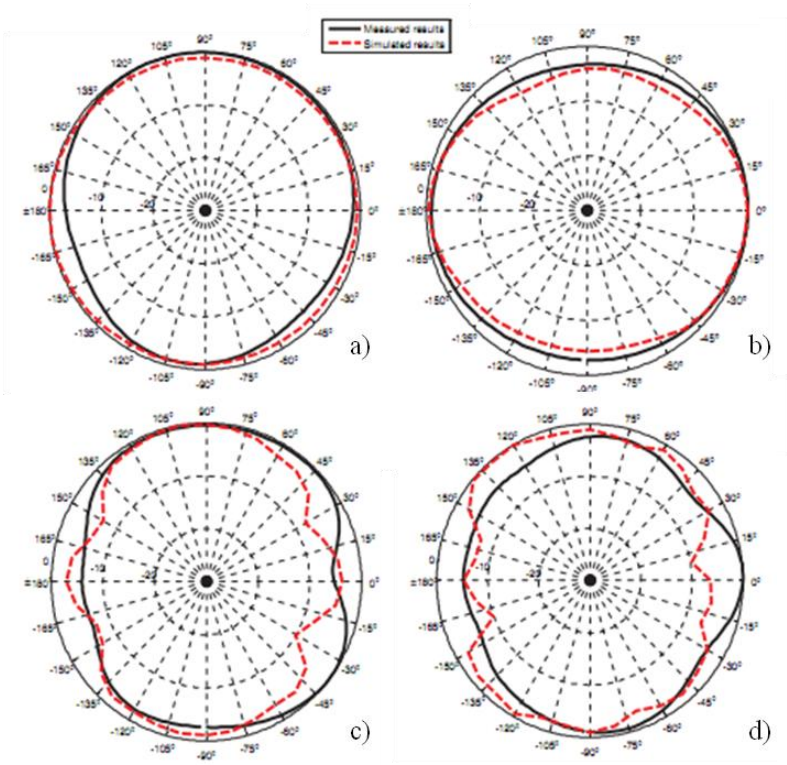

Figure 15. Radiation Patterns of the Elliptical Monopole Antenna in [23]
a) f = 3 GHz b) f = 5.6 GHz c) f = 8.8 GHz d) f = 11 GHz. Patterns are shown in the X-Y plane (Figure 14), or broadside.

3.2.2. Monopole with Ground Plane

Adding a ground plane is necessary in this project to produce a unidirectional beam. It also simplifies the biasing scheme of the varactors (Chapter IV section 4.3.2). Also, adding a ground plane requires only one FSS structure, instead of two. Investigations into the ground plane are discussed in this section. Figure 16 shows the diagram with the addition of a ground plane. The elliptical monopole antenna offers a slight modification from [23] (Figure 14) that are suitable to the application of this project and is further discussed in Chapter IV. The most important modification is the antenna is fed on the broadside of the ellipse; where [23] feeds the antenna on the small

side. The dimensions are shown in the figure, with the exclusion of the ground offset (u_{Ground}), which is discussed in this section.

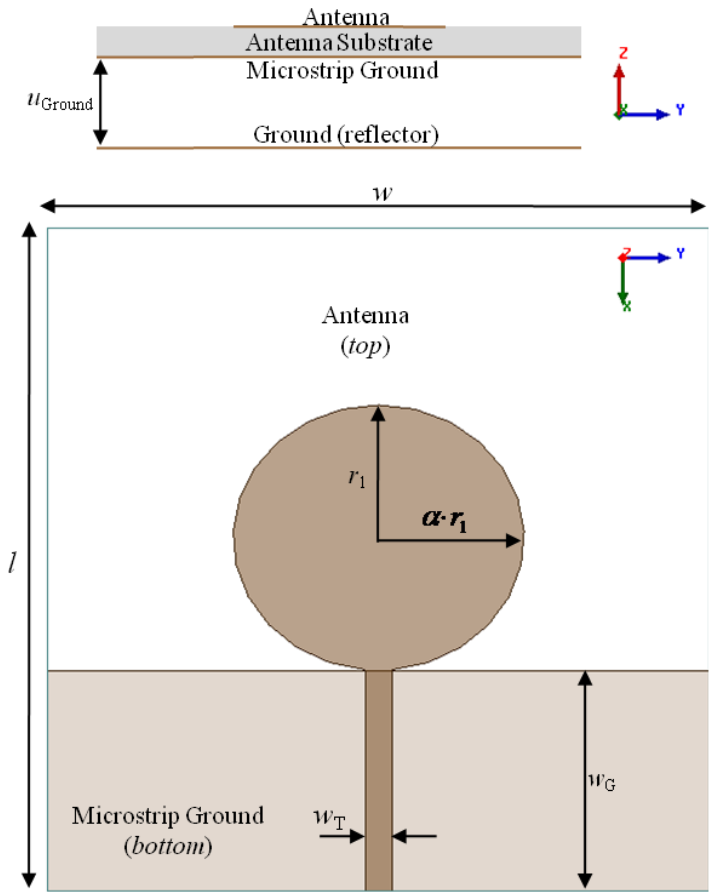

Parameter	Value
w	75 mm
l	75 mm
w_t	3 mm
r_1	15 mm
α	1.1
W_G	25 mm
u_{Ground}	N/A

Figure 16. Elliptical Monopole with Ground Plane

Figure 17 shows the effect of varying the ground distance from the bottom of the antenna substrate (denoted u_{Ground} in Figure 16). As the distance approaches 0 mm, the return loss resembles that of a patch antenna. Increasing the distance gradually improves the return loss of the monopole antenna. However, increasing the ground distance too much will result in a large structure and back radiation. Back radiation is undesired because the FSS will not filter this radiation because the FSS is placed above the antenna.

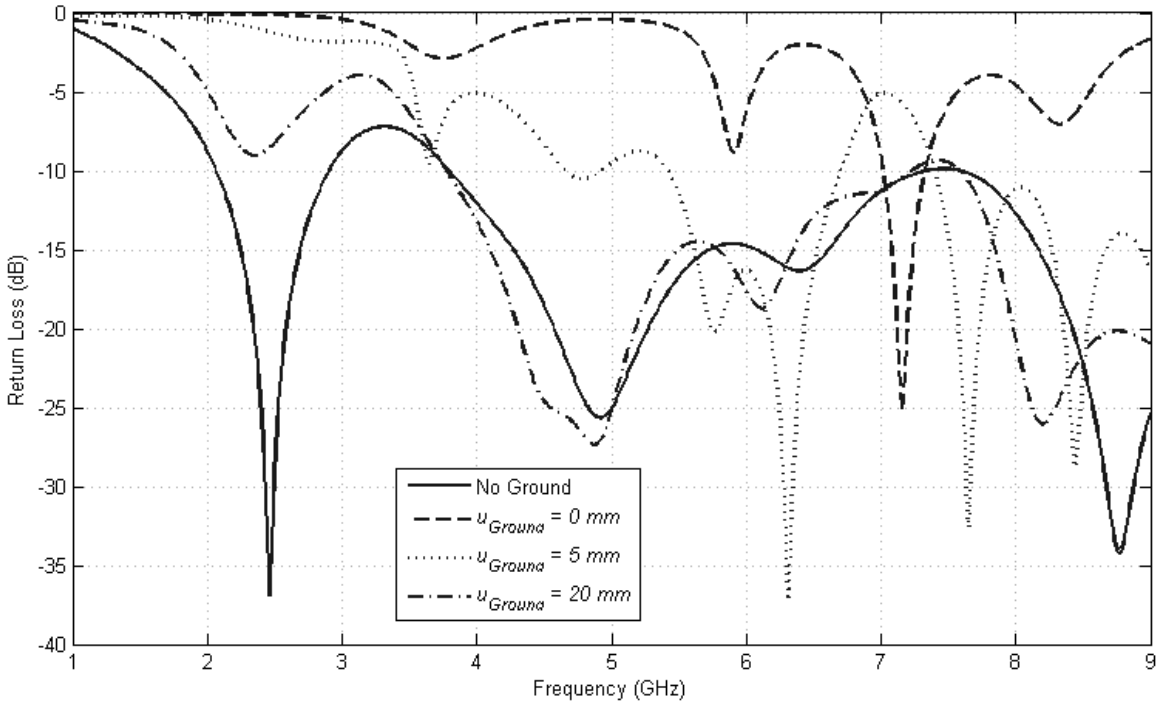

Figure 17. Return Loss (dB) of Various Ground Distances (u_{Ground})

3.2.3. Monopole with Aperture and Ground Plane

Investigation into improving the bandwidth while attaching a ground plane to the overall structure is discussed in this section. Authors of [27] propose using a "U" shaped tuning stub on a slot antenna to produce a 110% bandwidth in the UWB frequency range. This result led to research into adding an aperture behind the elliptical monopole antenna. Figure 18 shows the diagram of the elliptical antenna with an aperture and a ground plane. The aperture is placed under the antenna substrate, replacing the microstrip ground employed in section 3.2.1.

Parameter	Value
w	75 mm
l	75 mm
w_t	3 mm
l_t	20 mm
r_1	15 mm
α	1.1
w_A	41 mm
l_A	50 mm
u_{Ground}	5 mm

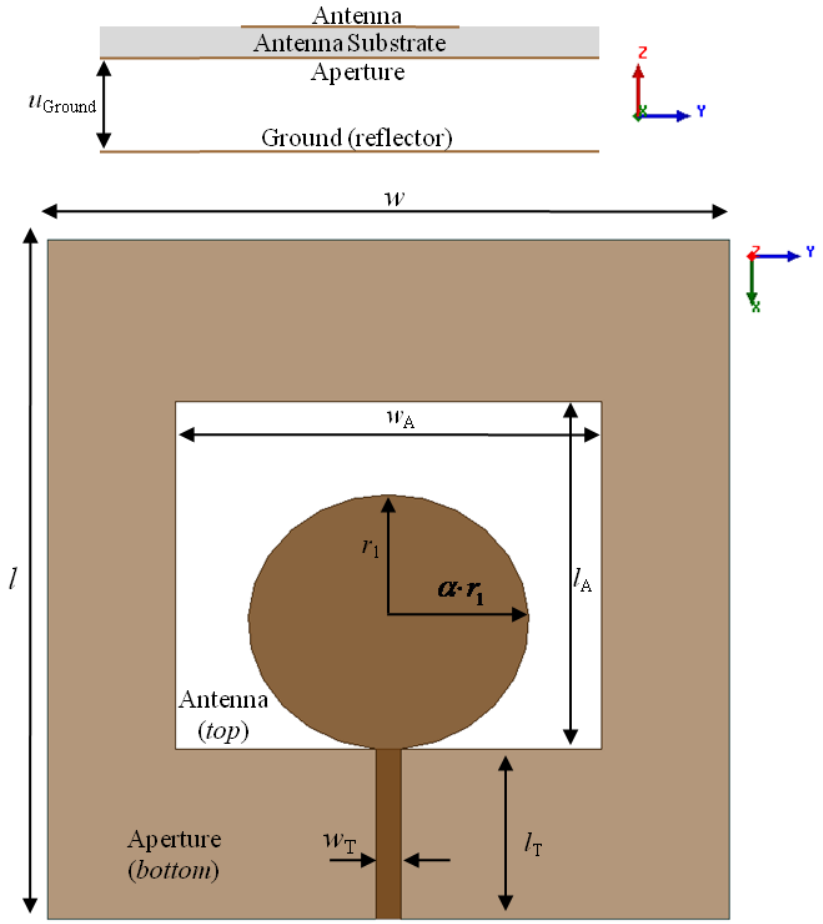

Figure 18. Elliptical Monopole with Aperture and Ground Plane

Figure 19 (top) shows the simulated return loss of the antenna in Figure 18 compared with the results in Figure 16. In both cases, the ground distance is 5 mm. As shown in the figure, the bandwidth is improved in the 5-7 GHz range. Further investigation into the design may yield a larger bandwidth. Figure 19 (bottom), demonstrates that the addition of the aperture does not negatively affect the desired broadside radiation.

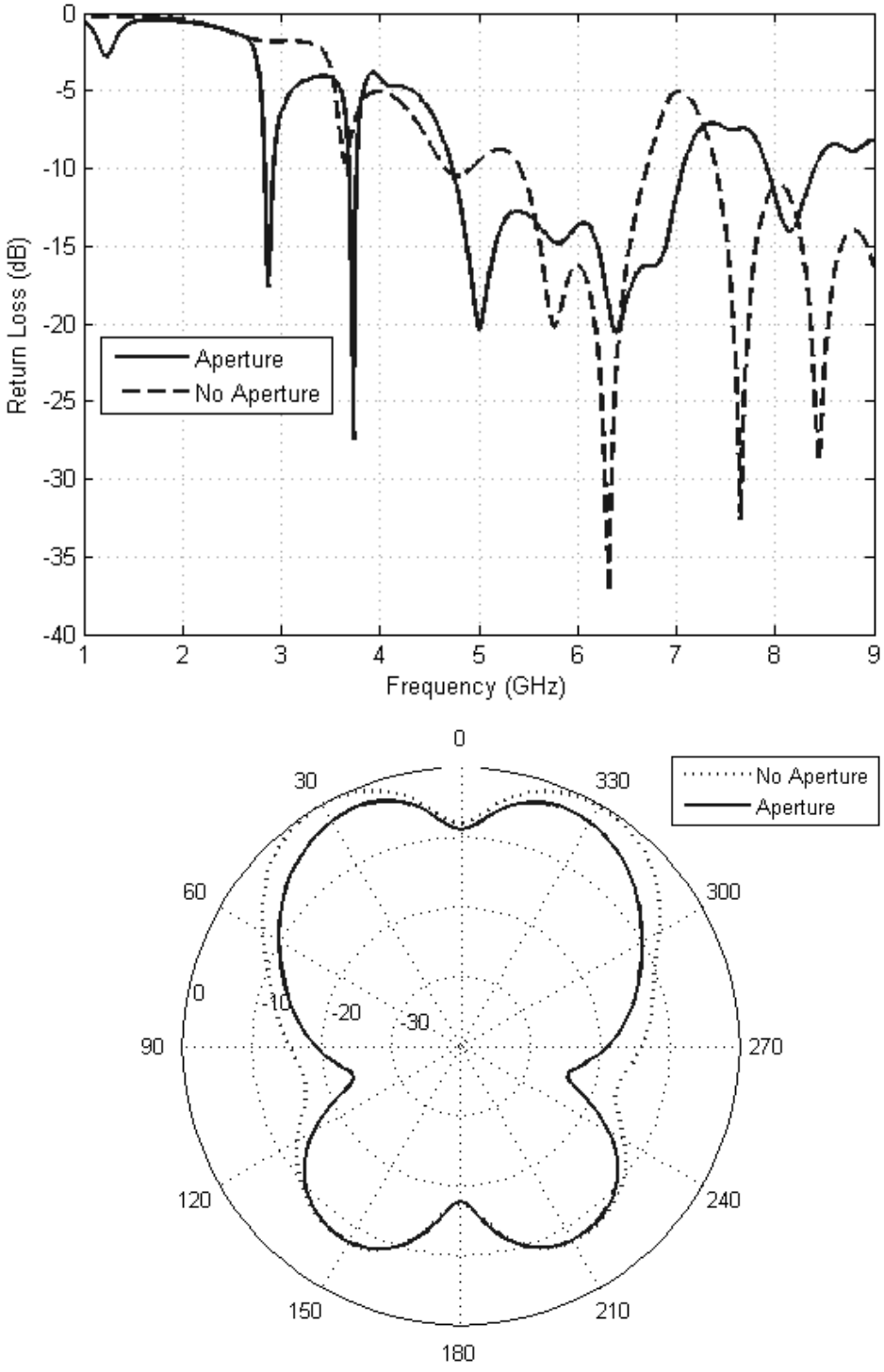

Figure 19. Return Loss and Y-Z Radiation Pattern of Elliptical Monopole
(top) return loss (bottom) radiation pattern. Antenna with and without Aperture Ground offset is 5 mm. Dimensions are given in Figure 16 and Figure 18

CHAPTER IV

PROPOSED DESIGN

4.1. Introduction

The proposed design and all of the elements of the design are discussed in this chapter. The FSS introduction in Chapter II and the UWB antenna introduction in Chapter III are extended to show the results of the designs that are employed by this project. This chapter will first discuss the independent design of the FSS, antenna, and varactors (sections 4.2.1, 4.2.3, and 4.2.2 respectively). Then the chapter will continue to simulation results with and without that addition of bias lines. Finally, the experimental results will be shown and compared with the simulated results.

4.2. Individual Components

This section will show the simulated results for the FSS and antenna. Also, the varactor considerations will be discussed. The sections are discussed independently; however, the components discussed depend on each other. The overall design with all components is simulated in section 4.3 and experimentally verified in section 4.4.

4.2.1. Frequency Selective Surface

The FSS employed in this project is shown in Figure 20. The parameters for the structure are shown in Table 3. The length and width are decided by the overall structure size. The ring radius is determined through simulations to provide a desirable tuning range for the selected antenna (Section 4.2.3 and Chapter III Section 3.2.2). The ring

thickness is 1 mm to allow the varactors to fit (Section 4.2.2). The capacitors simulating the varactors are on the left side of the rings as denoted by figure.

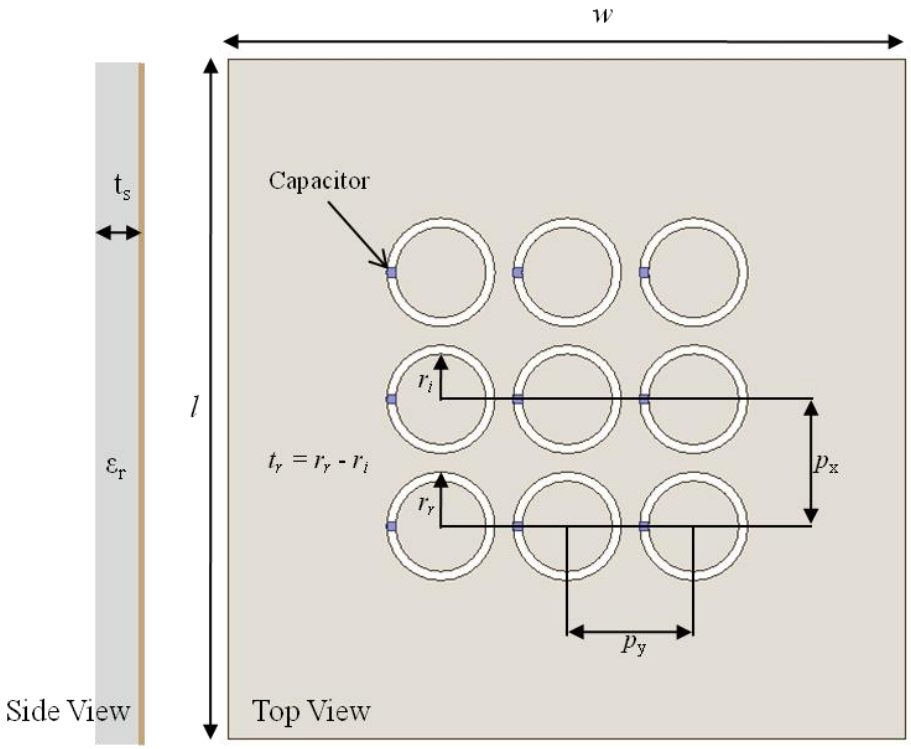

Figure 20. Frequency Selective Surface Employed

Table 2. Frequency Selective Surface Parameters

Parameter	Variable	Value
Ring Radius	r_r	6 mm
Ring Thickness	t_r	1 mm
Periodicity (x-direction)	p_x	14 mm
Periodicity (y-direction)	p_y	14 mm
Length	l	75 mm
Width	w	75 mm
Substrate Thickness	t_s	62 mil
Substrate Dielectric Constant	ε_r	2.33

Using the method discussed in Chapter II Section 3, the FSS is characterized with various capacitance values using HFSS. Figure 21 demonstrates the results of the simulated return loss for the FSS structure with various capacitances. The decision of the varactors within the selected values is discussed in section 4.2.2. However, given the capacitance range, a tuning range of 4.5 – 6.5 GHz is attainable. As discussed in Chapter II Section 3, the capacitance values may be increased; however, increasing the capacitance will result in smaller ring sizes. Eventually, however, the rings can no longer be realistically smaller to provide a sufficient resonance in the desired band.

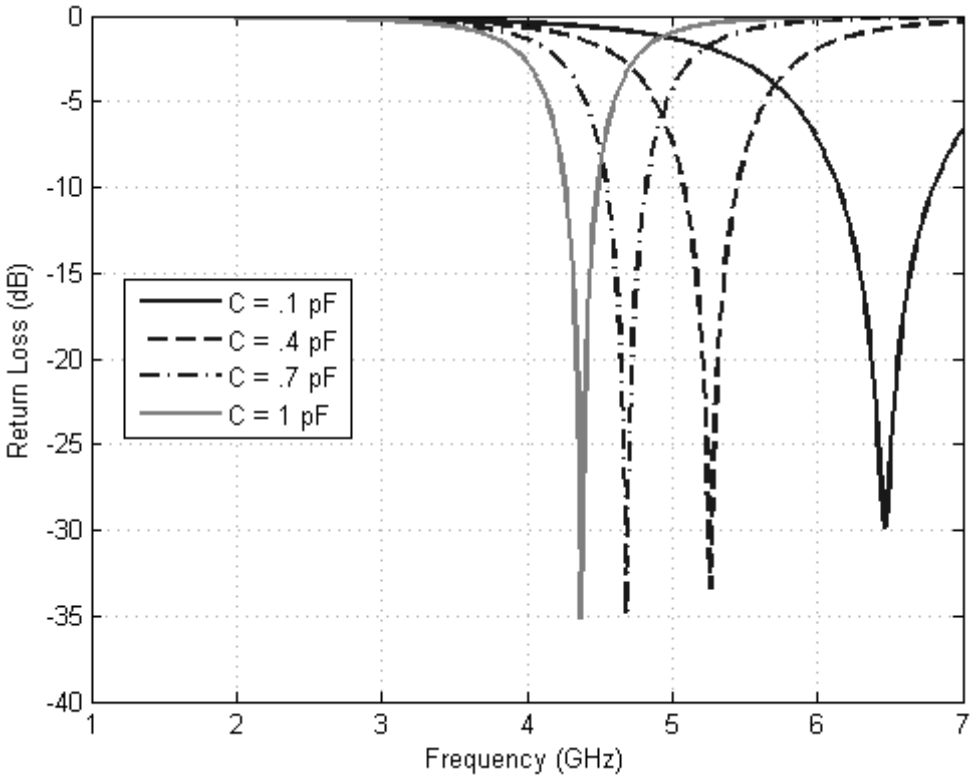

Figure 21. Simulated Return Loss of FSS with Various Capacitance Values

4.2.2. Varactors

Varactor selection within the 0.1 – 1 pF range is difficult; with the varactors being quite expensive. The varactors employed, provided by Aeroflex Metelics, are MGV-125-08-0805. The varactors are hyperabrupt, gallium arsenide (GaAs) diodes with the specifications shown in Table 3 [28]. The varactors are provided in a convenient 0805 package. The measured capacitance of the 14 varactors provided by Aeroflex Metelics is shown in Figure 22. The figure shows the four measured points of the varactors (2, 4, 12, and 20 V), with the average of each capacitance given on the figure.

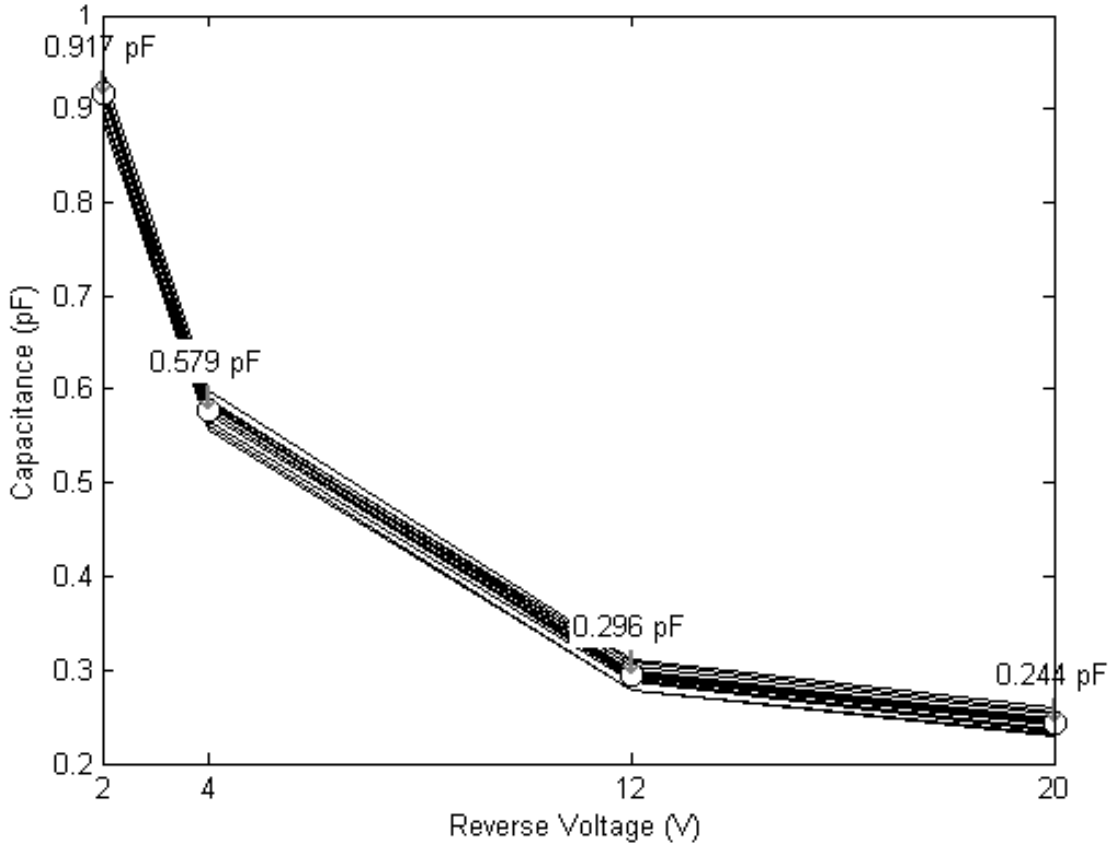

Figure 22. Measured Varactor Capacitance versus Reverse Voltage [28]

Table 3. Varactor Parameters [28]

Parameter	Value
Γ	1.25±10 %
C_T (4 V)	0.3 - 0.42 pF (0.36 pF nominal)
Tuning Ratio (2 – 12 V)	4.1 (Typical)
Tuning Ratio (2 – 20 V)	7.0 (Typical)
Q	3000
C_p	.06 pF
L_p	.4 pF

Modeling the varactors in HFSS is not necessary because the capacitance can be inferred from Figure 22 given the reverse bias voltage. However, crude curve fitting using a Las Vegas algorithm (similar to Monte Carlo) to solve the variables in equation (1) was implemented to model the varactors [29]. The MATLAB code for the Las Vegas algorithm generated solution is given in Appendix A. The parameters of equation (1) are shown in Table 4. The capacitance at 0 V is given by the Aeroplex Metelics by measurement and was shown to be around 2.4 pF. Γ is given by the varactor datasheet. The junction voltage is given by the process, for GaAn V_j is 1.3 V and 0.7 V for silicon [29].

$$C = \frac{C_0}{\left(1+\frac{V}{V_j}\right)^m} + C_p \tag{1}$$

Table 4. Variable Definitions in Equation (1) [28]

Parameter	Variable	Value	Tolerance
Capacitance at 0 V	C_0	2.4 pF	± 10%
Junction voltage	V_j	1.3 V	± 10%
Γ	m	1.25	± 10%
Parasitic Capacitance	C_p	0.06 pF	N/A

The Las Vegas algorithm assumes all the parameters values in Table 4 are within the tolerance, except the parasitic capacitance. Also, the simulation uses the average value of the capacitances given by Figure 22. The result of the simulation is shown in Figure 23. The average varactor capacitance fits the curve within ±0.008 pF. The variables obtained from the simulation are shown in Table 5 and are used in the subsequent sections for the HFSS simulations.

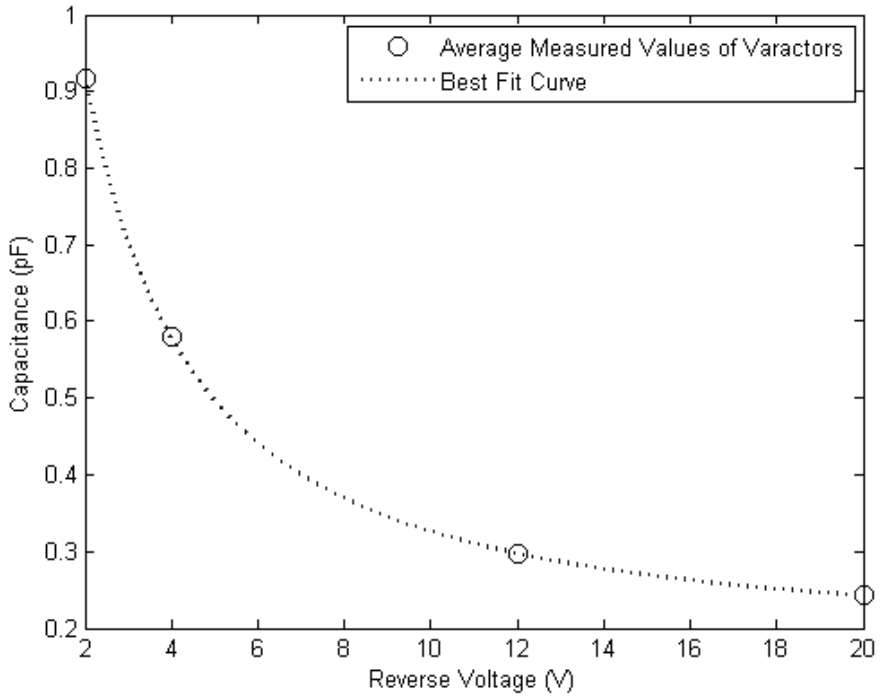

Figure 23. Las Vegas Best Fit Curve for Varactor Capacitance versus Reverse Voltage

Table 5. Results from Las Vegas Varactor Curve Fitting

Parameter	Variable	Expected Value	Value From Las Vegas	Deviation
Capacitance at 0 V	C_0	2.4 pF	2.3907 pF	0.39%
Junction voltage	V_j	1.3 V	1.4108 V	8.53%
Γ	m	1.25	1.3365	6.92%
Parasitic Capacitance	C_p	0.06 pF	0.1793 pF	199%

4.2.3. Elliptical Monopole Antenna

The UWB antenna employed in this project is the exact antenna discussed in Chapter III Section 3.2.2. The antenna is an elliptical monopole antenna with a ground plane placed behind the structure to prevent back radiation allow for easy biasing of the varactors employed on the FSS.

4.3. Simulated Results

The design is simulated using Ansoft's HFSS prior to physically constructing the model. This chapter discusses the simulated results and two models. Section 4.3.1 discusses the simulated design with no bias lines and section 4.3.2 shows the simulated results with the addition of the bias lines. The following sections build on section 4.2 which demonstrated the individual components.

4.3.1. Simple Design

This section discusses the simulated results of the UWB fed, tunable FSS. The simple model is shown in Figure 24. These results exclude the addition of the bias lines that would exist when the structure is constructed (discussed in section 4.3.2). The parameters for the structure are listed in Table 6. The optimum placement of the varactors is decided through simulation and placed where a maximum electric field distribution occurs as discussed in Chapter II, section 2.3.2.

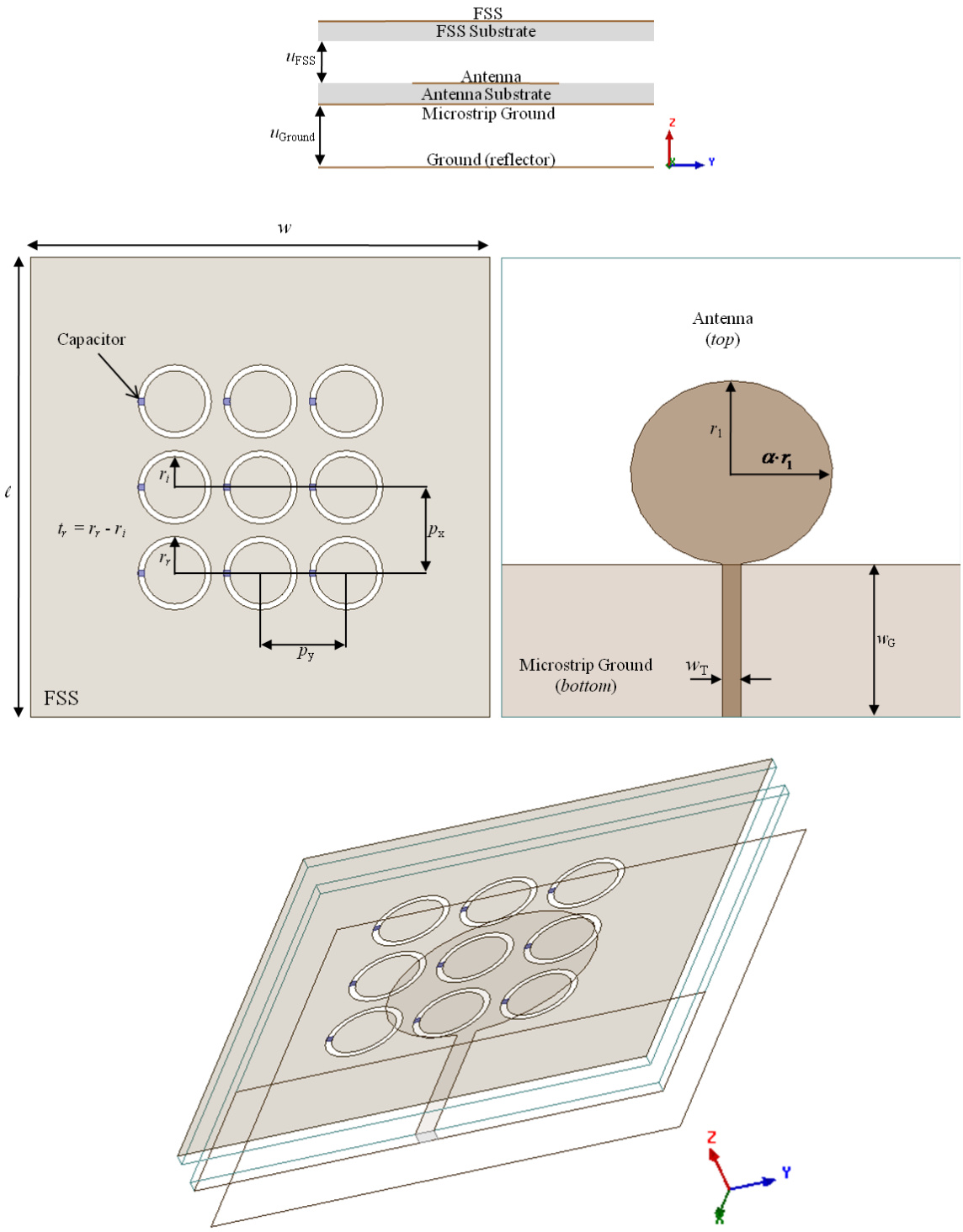

Figure 24. Diagram for Simple UWB Fed, Tunable FSS

Table 6. Parameters for Simulated UWB Fed, Tunable FSS

Parameter	Variable	Value
FSS Ring Radius	r_r	6 mm
FSS Ring Thickness	t_r	1 mm
FSS Periodicity (x-direction)	p_x	14 mm
FSS Periodicity (y-direction)	p_y	14 mm
Antenna Radius	r_1	15 mm
Antenna Radial Ratio	α	1.1
Antenna Feed Width	w_T	3 mm
Microstrip Ground width	w_G	25 mm
FSS Distance	u_{FSS}	1 mm
Ground Distance	u_{Ground}	20 mm
Length	l	75 mm
Width	w	75 mm
Substrate Thickness	N/A	62 mil
Substrate Dielectric Constant	N/A	2.33

Using the equation (1) and the variables listed in Table 5, the capacitor is simulated similar to the varactor discussed in section 4.2.2. Figure 25 shows the return loss of various reverse voltage values of the simulated varactors. The tuning range for this structure is around 4.5 – 5.5 GHz. Larger reverse voltages produce increases in the resonant frequency of the structure. The resonance around 5.8 GHz is a cavity resonance mode and is reduced with the inclusion of the bias lines (section 4.3.2). The discontinuous tuning range will be discussed in section 4.5 with the comparison of results.

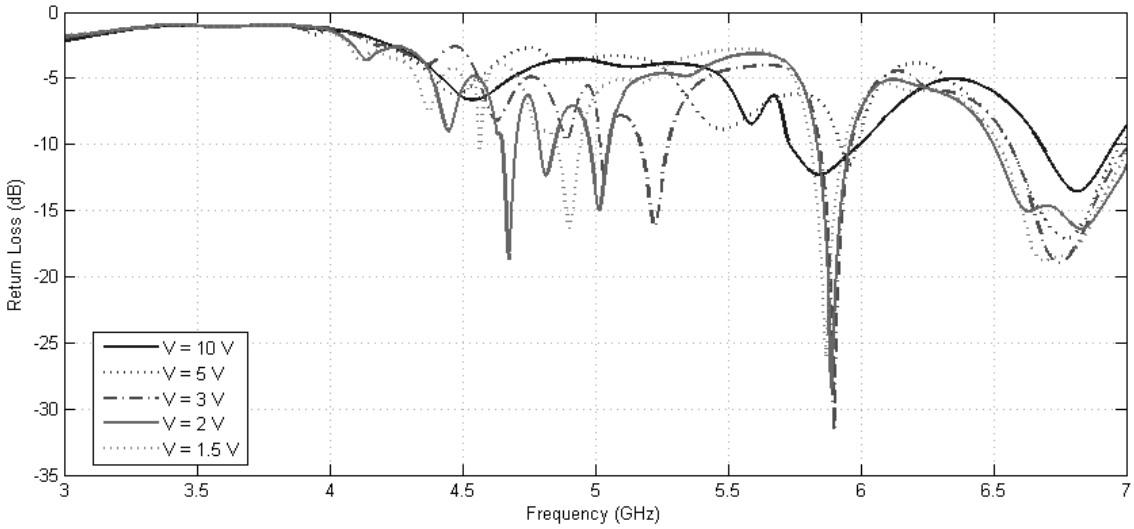

Figure 25. Simulated Return Loss of Various Varactor Reverse Voltages

The return loss and radiation patterns for a reverse voltage of 2 V are shown in Figure 26; and Figure 27 for a reverse voltage of 3 V. Both return loss plots (a. in both figures) show multiple resonant points. The radiation pattern is shown where the resonance is the strongest. For the reverse voltage of 2 V, this resonance occurs at 4.675 GHz; and 5.22 GHz for the 3 V case. The radiation patterns show the cross and co-polarizations of both the X-Z and Y-Z planes. The results show the structure is not linearly polarized. However, the monopole antenna produces linearly polarized waves. Lastly, the figures show the total radiation power from the structure. The results of the total radiation demonstrate that the structure is producing some beam steering. The beam steering application is proposed as a suggested improvement in Chapter V.

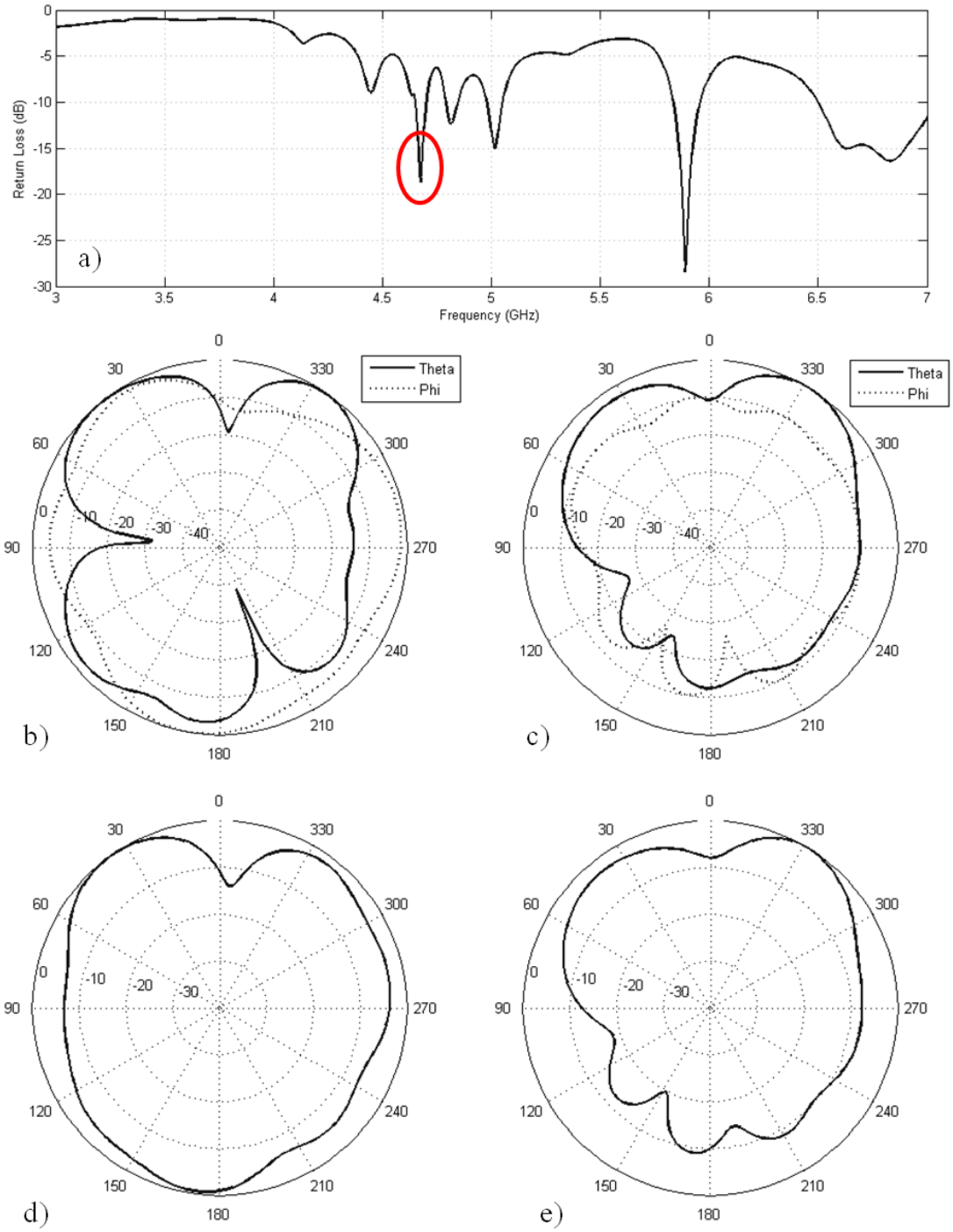

Figure 26. Return Loss and Y-Z Radiation Patterns at 4.675 GHz of Simple Structure Where Reverse Voltage is 2 V
a) Return loss with 4.675 GHz resonance circled b) cross and co polarization in X-Z Plane c) cross and co polarization in Y-Z plane d) total radiation X-Z plane e) total radiation in Y-Z plane. Radiations patterns are in normalized dB. Refer to Figure 24 for plane reference.

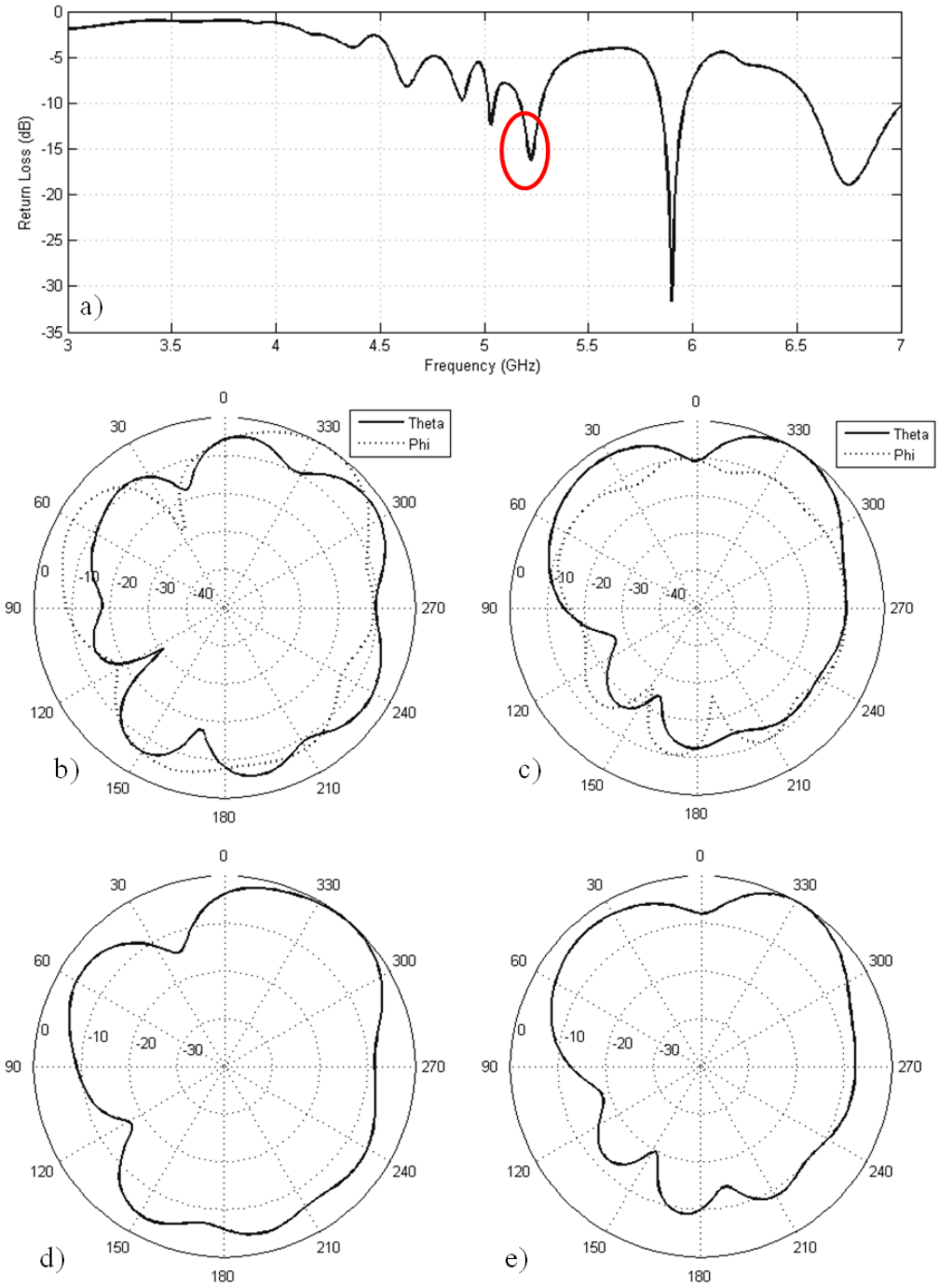

Figure 27. Return Loss and Y-Z Radiation Patterns at 5.22 GHz of Simple Structure Where Reverse Voltage is 3 V
a) Return loss with 5.22 GHz resonance circled b) cross and co polarization in X-Z Plane c) cross and co polarization in Y-Z plane d) total radiation X-Z plane e) total radiation in Y-Z plane. Radiations patterns are in normalized dB. Refer to Figure 24 for plane reference.

4.3.2. Design with Bias Lines

The final design discussed in section 4.4 includes bias lines to control the varactor reverse voltage. These bias lines are implemented in HFSS and simulated. Figure 28 shows the bias lines. Each varactor has a bias line; consequently each ring has a bias line that runs directly to the center of the inner ring. The lines are extended through the antenna to the ground plane underneath. The dimensions of the antenna and rings remain the same (Figure 24 and Table 6).

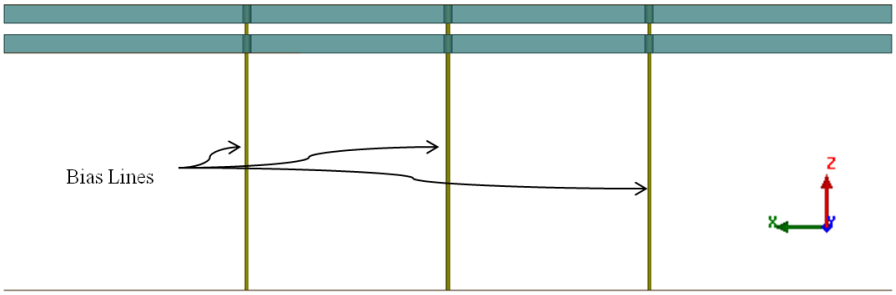

Figure 28. Bias Lines

The return loss for various reverse voltages is shown in Figure 29. The resonances are circled in the figure for clarity. As the varactor reverse voltage increases, the resonant frequency of the antenna and FSS structure increases. The results show a frequency tuning of just over 1 GHz. The surface wave radiation still exists around 6.5 – 7 GHz; however, the surface wave radiation around 6 GHz in the simple model (Figure 25) has disappeared. Also, the structure appears to have a discontinuity in the tuning range around 4.5 GHz. A similar discontinuity exists in the experimental prototype (section 4.4.1), though at a lower frequency.

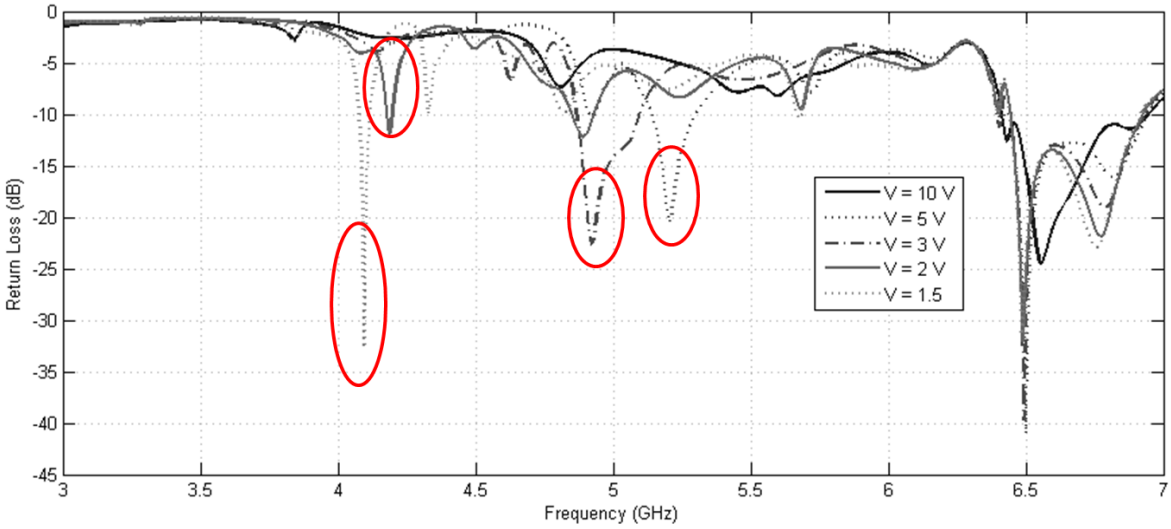

Figure 29. Return Loss for Various Reverse Voltages with Bias Lines
The resonances are circled from left to right 1.5 V, 2 V, 3 V, and 5 V. 10 V resonance is not present.

Figure 30 shows the return loss of the FSS and UWB structure with the varactors biased at 3 V. The figure also shows the radiation patterns at 4.9 GHz; which is where the resonance occurs. As mentioned in the previous section, the radiation patterns show the structure is not linearly polarized. Significant back radiation still exists from the structure; however, the addition of a larger reflector is investigated in section 4.4.4 which produces an improvement in back-to-front radiation.

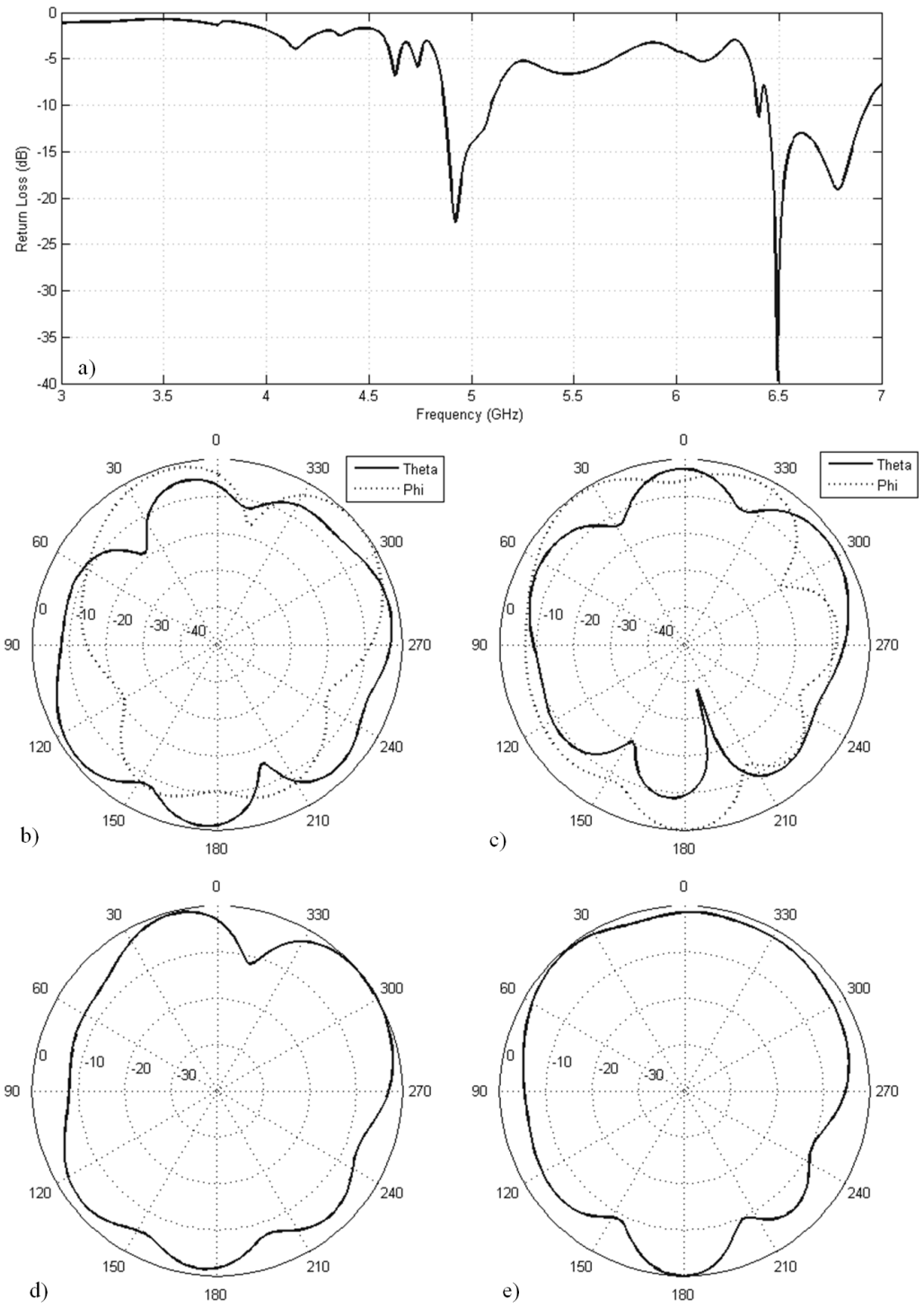

Figure 30. Return Loss and Radiation at 4.9 GHz with a Reverse Voltage of 3 V
a) Return loss b) cross and co polarization in X-Z Plane c) cross and co polarization in Y-Z plane d) total radiation X-Z plane e) total radiation in Y-Z plane. Radiations patterns are in normalized dB. Refer to Figure 24 for plane reference.

4.3.3. Other Attempted Designs

Other modifications to the simple structure were attempted to silence the surface wave radiation around 6 GHz (in the simple design). Enclosing the structure by placing conductors on all four sides was attempted first. No desirable results were produced as the cavity resonance of the structure dominated. Absorbing material was added to try to reduce the cavity resonances; however, no desirable results appeared in this design either. Lastly, the structure was opened with absorbing material placed on the sides – still no desirable results. The design that produces the best results is the simple design with bias lines (previous section) and serves as the prototype in Section 4.4.

4.4. Experimental Results

The prototype used for experimental results is shown in Figure 31. All components of the prototype are labeled in the figure. The dimensions of the structure are identical to Figure 24 and Table 6. The structure employs an SMA connector to connect to a network analyzer. The FSS and ground distances may be modified by adjusting the plastic screws and bolts on the corners. The varactor ground is provided by soldering a wire on the surface. The bias voltage for the varactors is given on the underside of the ground, as the bias lines pierce the ground and are soldered on the back side. The bias lines are intentionally too long to provide room for adjustment of the ground plane and FSS. The bias lines also pass through the antenna plane and are soldered to the center of the FSS rings using vias. The cathodes of the varactors are soldered to the inner ring and the anodes are soldered outside the rings (to the varactor ground).

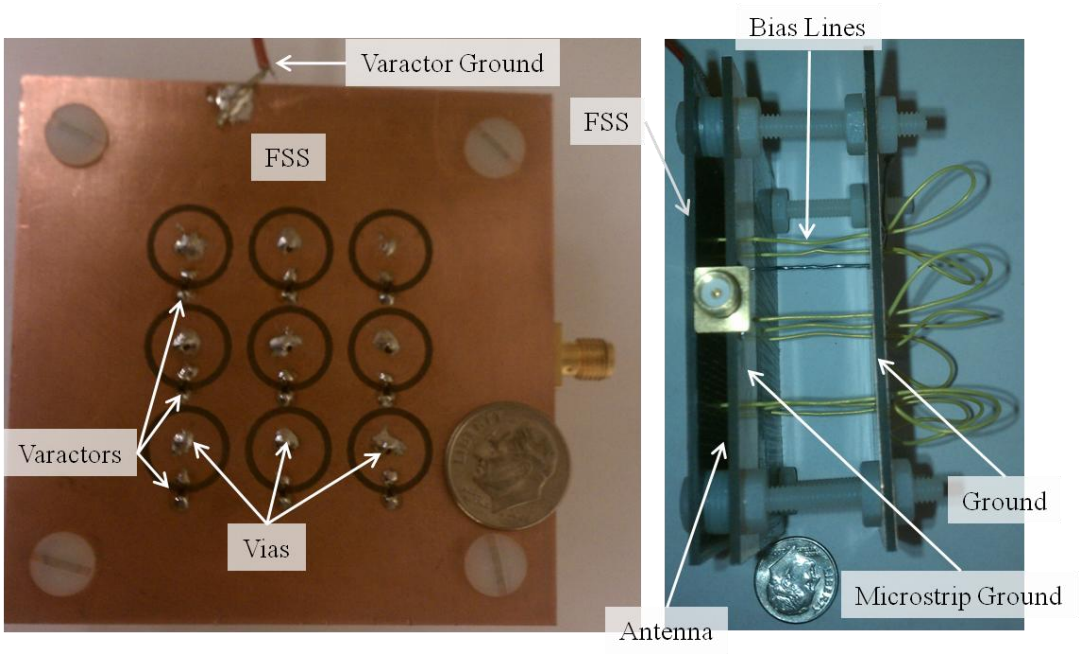

Figure 31. Prototype

The following sections will work to demonstrate the tunability of the UWB fed FSS structure in Figure 31. Section 4.4.1 demonstrates the tuning of the structure with dimension in Table 6. Section 4.4.2 will discuss the placement of the ground from the antenna; section 4.4.3 will discuss the placement of the frequency selective surface. Both sections will discuss how the placements affect the return loss and tunability of the structure. Finally, section 4.4.4 will demonstrate the radiation from the FSS and UWB structure.

4.4.1. Tuning

The primary concern of this research is the tunability of FSS and UWB antenna structure. The dimensions of the structure are given in Figure 24 and Table 6. The tuning

is shown in Figure 32. The figure demonstrates as the reverse voltage of the varactors increases, the resonant frequency increases.

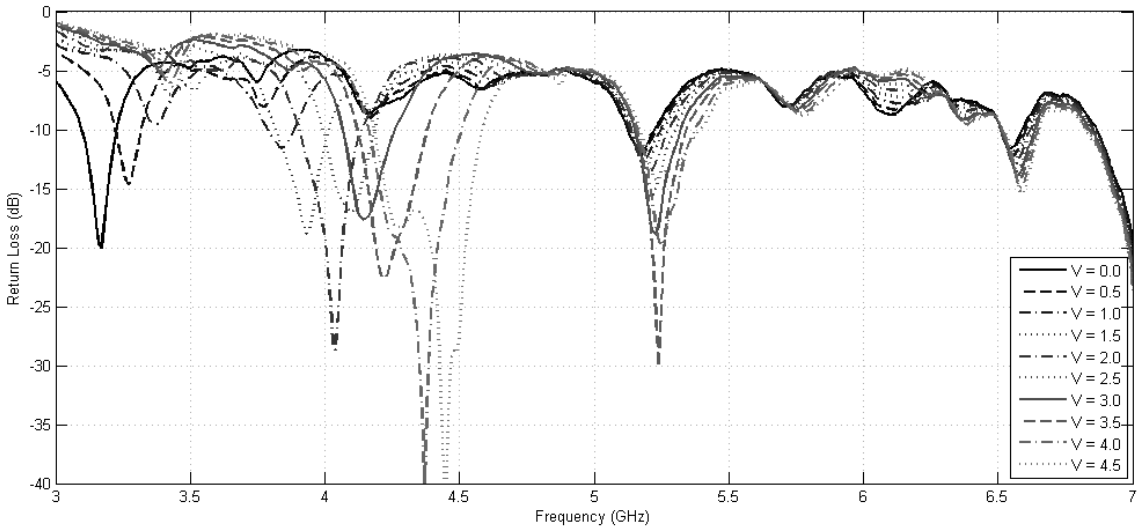

Figure 32. Experimental Verification of Tuning

The tuning is discontinuous around 3.5 GHz because the antenna does not have sufficient return loss at 3.5 GHz (Figure 17). Also, when the reverse voltage approaches 3.5 – 4.5 V, the resonance begins to split. Figure 33 demonstrates the resonance splitting as the voltage increases. However, if the voltage remains between 0 – 4.5 V, the resonance splitting is not as drastic and will yield a tuning range from 3.2 – 4.5 GHz (neglecting the 3.5 GHz null). The resonance splitting and 3.5 GHz null are given as suggested improvements in the conclusion (Chapter V).

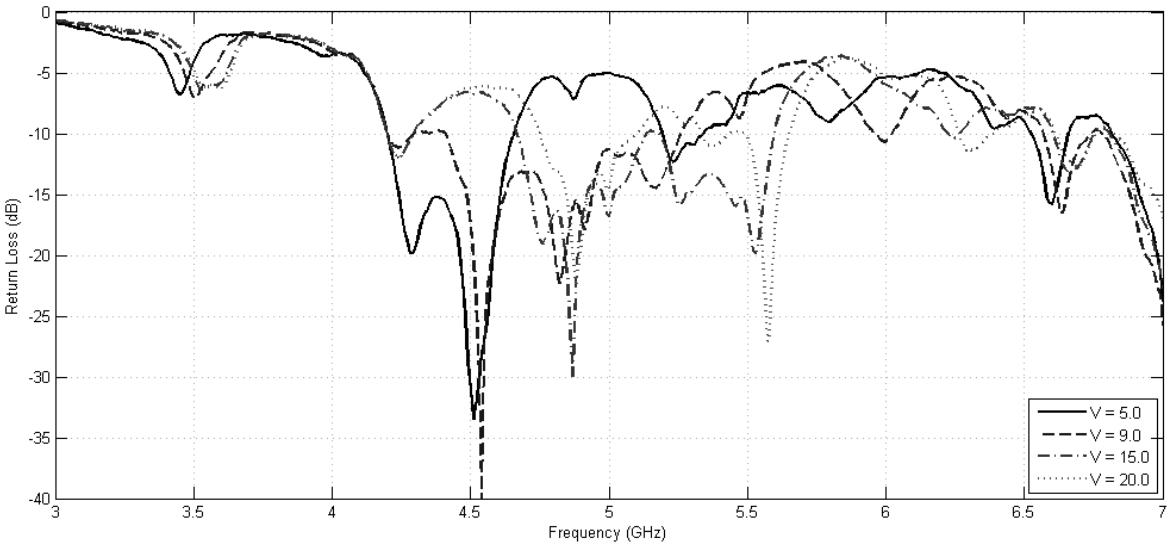

Figure 33. Demonstration of resonance splitting

4.4.2. Ground Distance

The placement of the ground is crucial, as discussed previously in Chapter III section 3.2.2. The placement of the ground is easily modified experimentally. Figure 34 and Figure 35 summarize the results. The FSS distance is constant (1 mm), and the return loss for various reverse voltages is shown in the figures. As demonstrated in the figures, if the ground distance is small and the reverse voltage is increased, the resonances become scattered and less defined. The figures also demonstrate that a ground distance of 20 mm is optimum; which is used for the tuning range demonstration in the previous section and in the following sections.

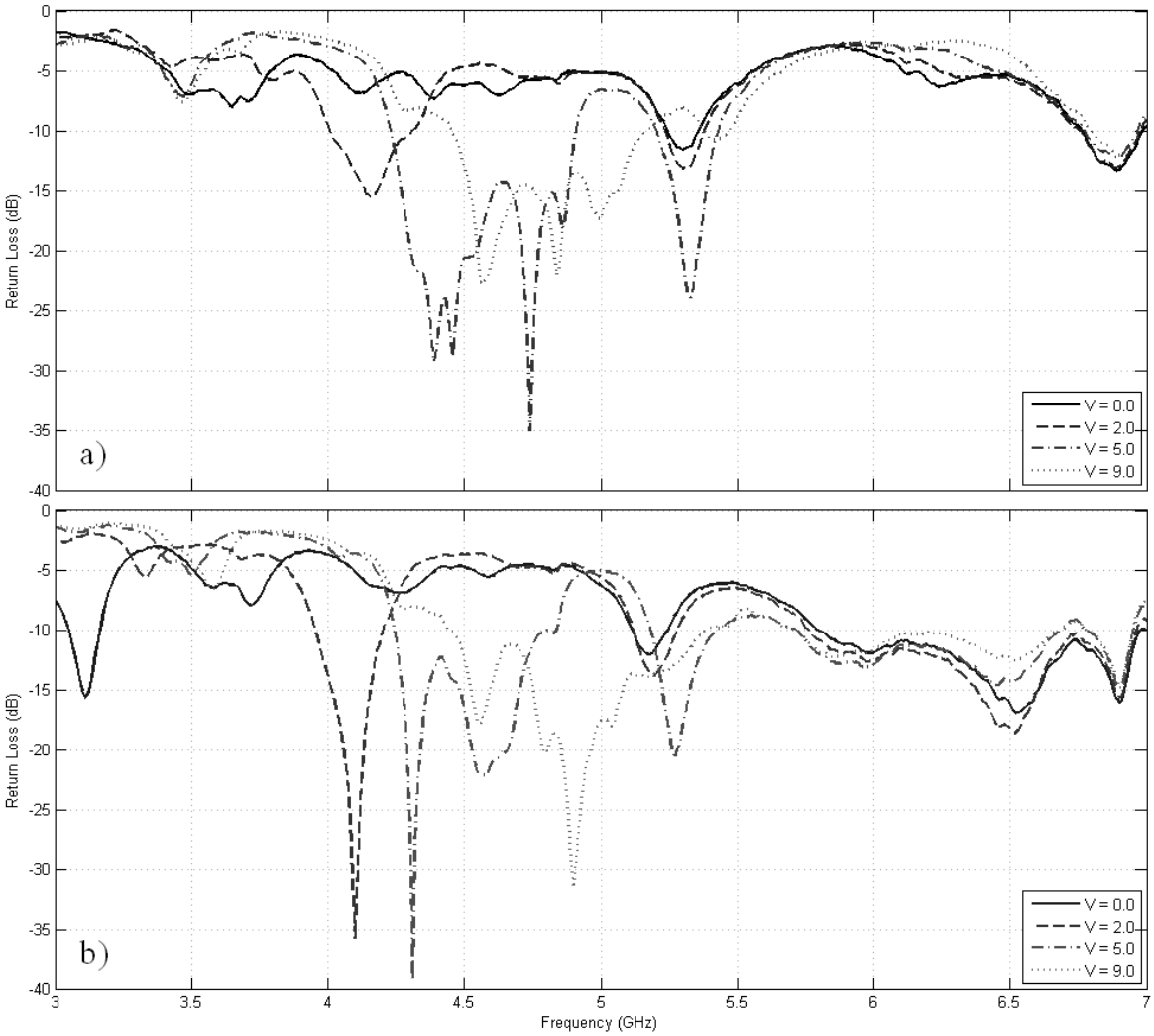

Figure 34. Return Loss for Ground Distances of 10 mm and 15 mm
a) 10 mm b) 15 mm u_{FSS} = 1 mm (Refer to Figure 24)

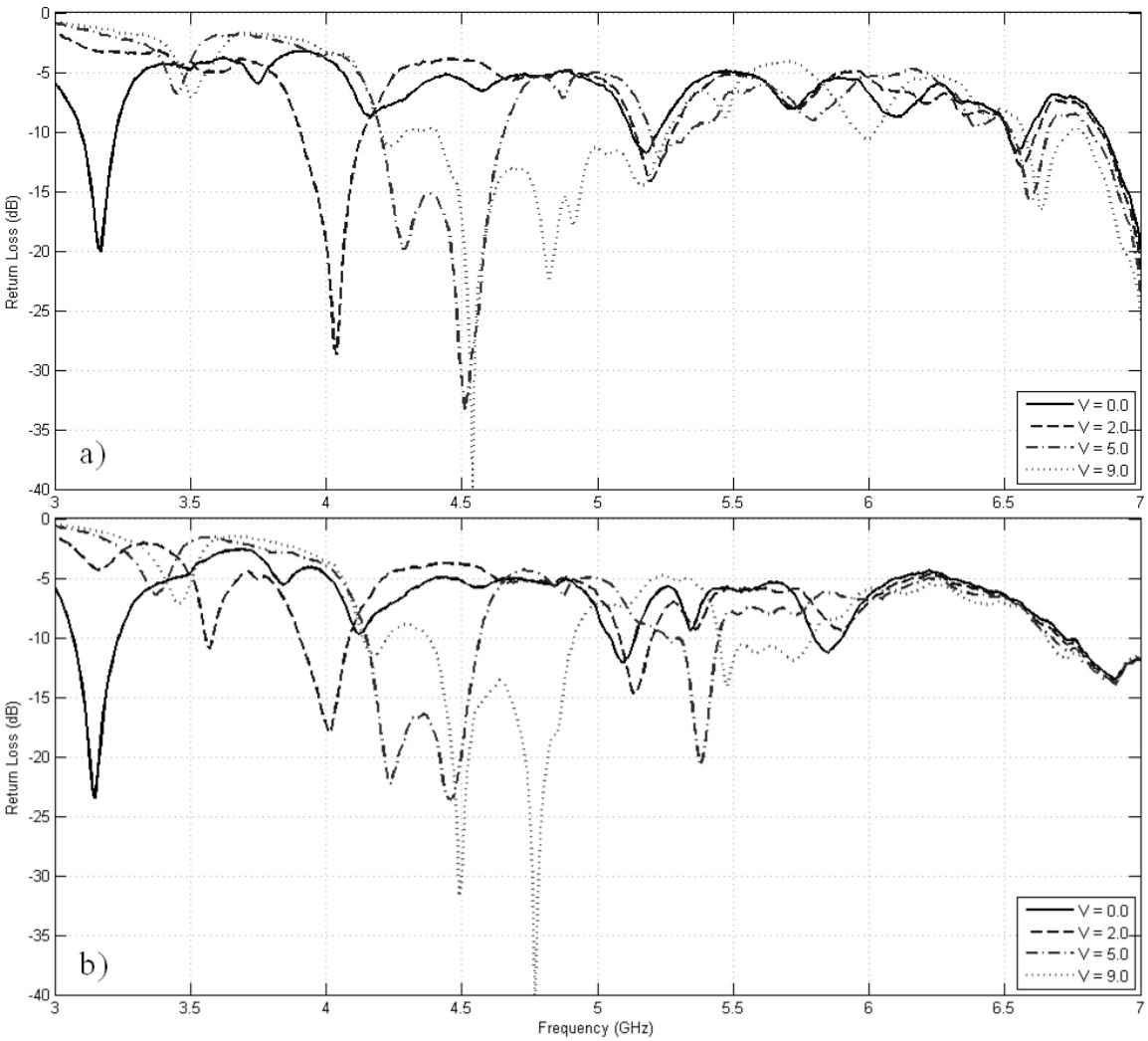

Figure 35. Return Loss for Ground Distances of 15 mm and 20 mm
a) 20 mm b) 25 mm u_{FSS} = 1 mm (Refer to Figure 24)

4.4.3. FSS Distance

The distance from the FSS and antenna also places a crucial role. The tuning demonstrated in Figure 34 is shown with an FSS distance of 1 mm. Figure 36 shows the return loss when the FSS is placed 5 mm away from the antenna. The figure can be compared to Figure 34 c) (where the ground distance is the same). The figure demonstrates undesirable effects of tuning. When V = 0 V, a resonance appears around

4.5 GHz which is not present when the FSS is 1 mm away. A reverse voltage of 9 V does not produce a resonance. Also, the resonances are not as well defined.

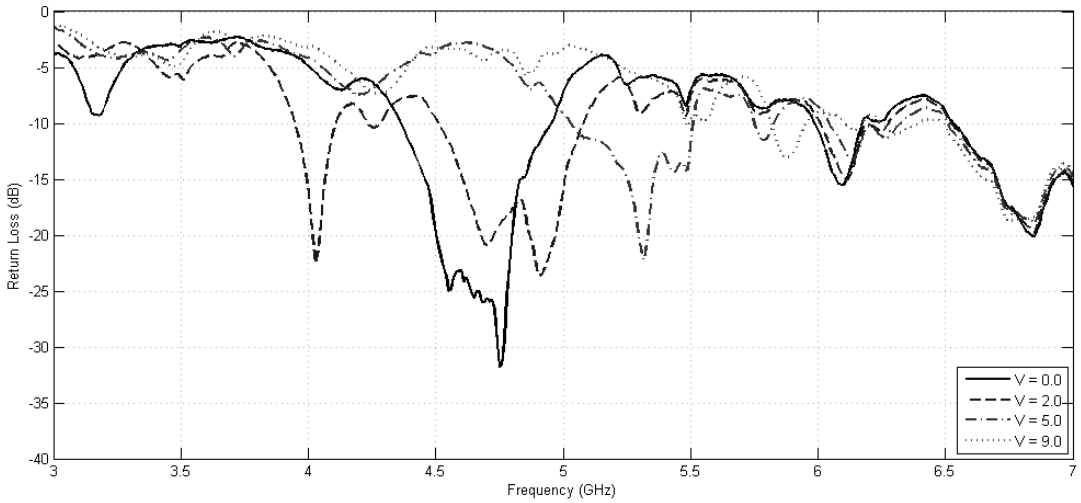

Figure 36. Return Loss of Various Reverse Voltages where u_{FSS} = 5 mm; u_{Ground} = 20 mm

4.4.4. Radiation

The radiation patterns when the varactors are biased at 2 V are shown Figure 37; patterns at a reverse bias of 3 V are shown in Figure 38. There is no clear distinction between the cross and co-polarization in the patterns; therefore, the total power distribution is shown in the figures. As mentioned in the previous sections, the structure is no longer linearly polarized. The cross and co-polarization is provided as a suggested improvement in Chapter V. No attempts are made to improve the cross and co-polarization.

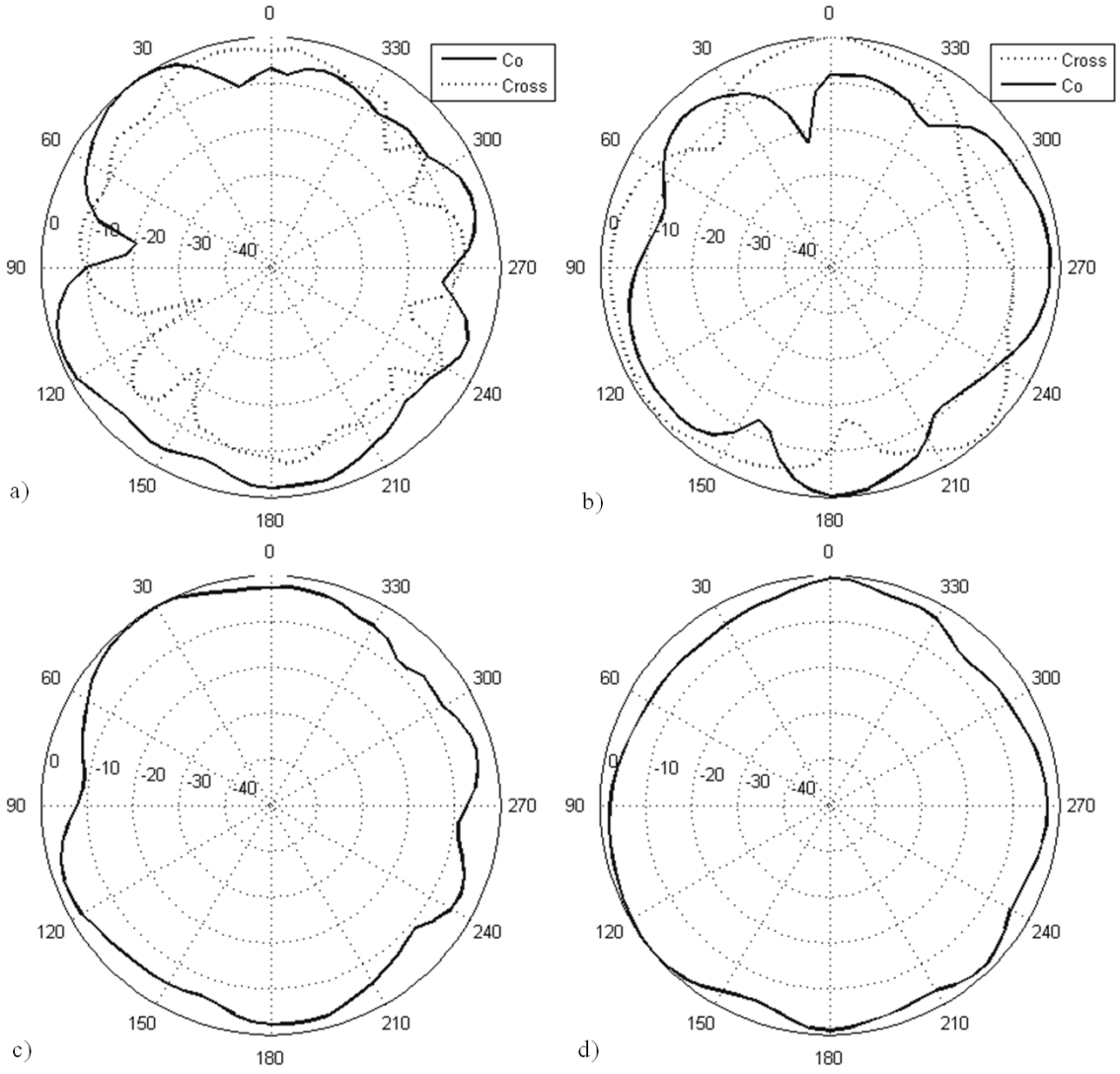

Figure 37. Radiation Patterns When Varactors are Biased at 2 V Resonance occurs at 4.02 GHz (Figure 32) a) X-Z plane b) Y-Z plane c) Total Radiation X-Z plane d) Total Radiation Y-Z plane. Refer to Figure 24 for plane reference. Patterns are normalized dB.

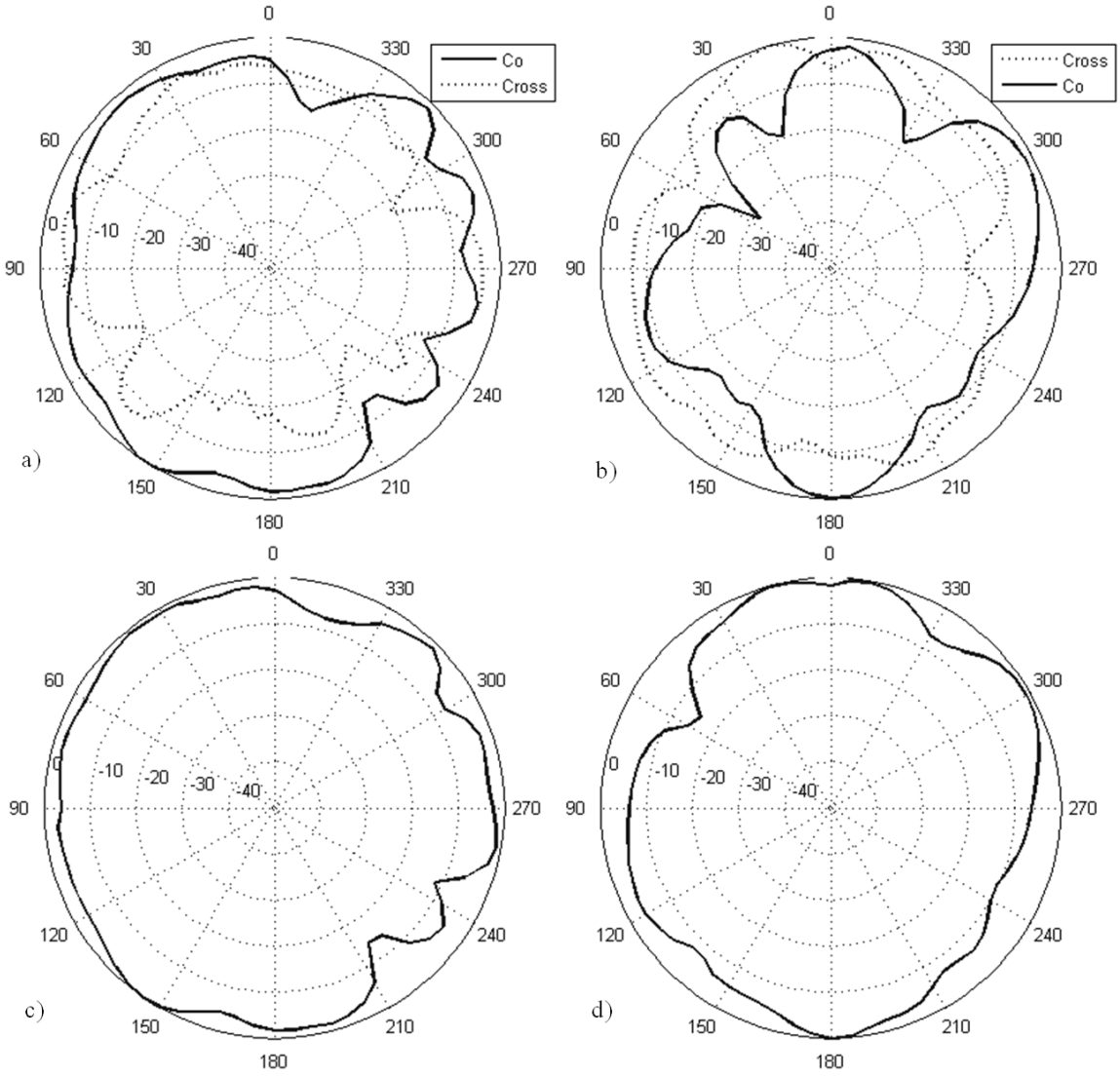

Figure 38. Radiation Patterns When Varactors are Biased at 3 V Resonance occurs at 4.17 GHz (Figure 32) a) X-Z plane b) Y-Z plane c) Total Radiation X-Z plane d) Total Radiation Y-Z plane. Refer to Figure 24 for plane reference. Patterns are normalized dB.

Because the back radiation is still significant, a larger ground plane is placed behind the antenna structure. The ground placed is placed behind the bias wires on the ground plane (Figure 31). The results with the ground plane are shown in Figure 39

(reverse bias of 2 V) and Figure 40 (reverse bias of 3 V). The results improve the back-to-front ratio to almost 10 dB in all planes. The addition of a larger ground plane is provided as a suggested improvement in Chapter V.

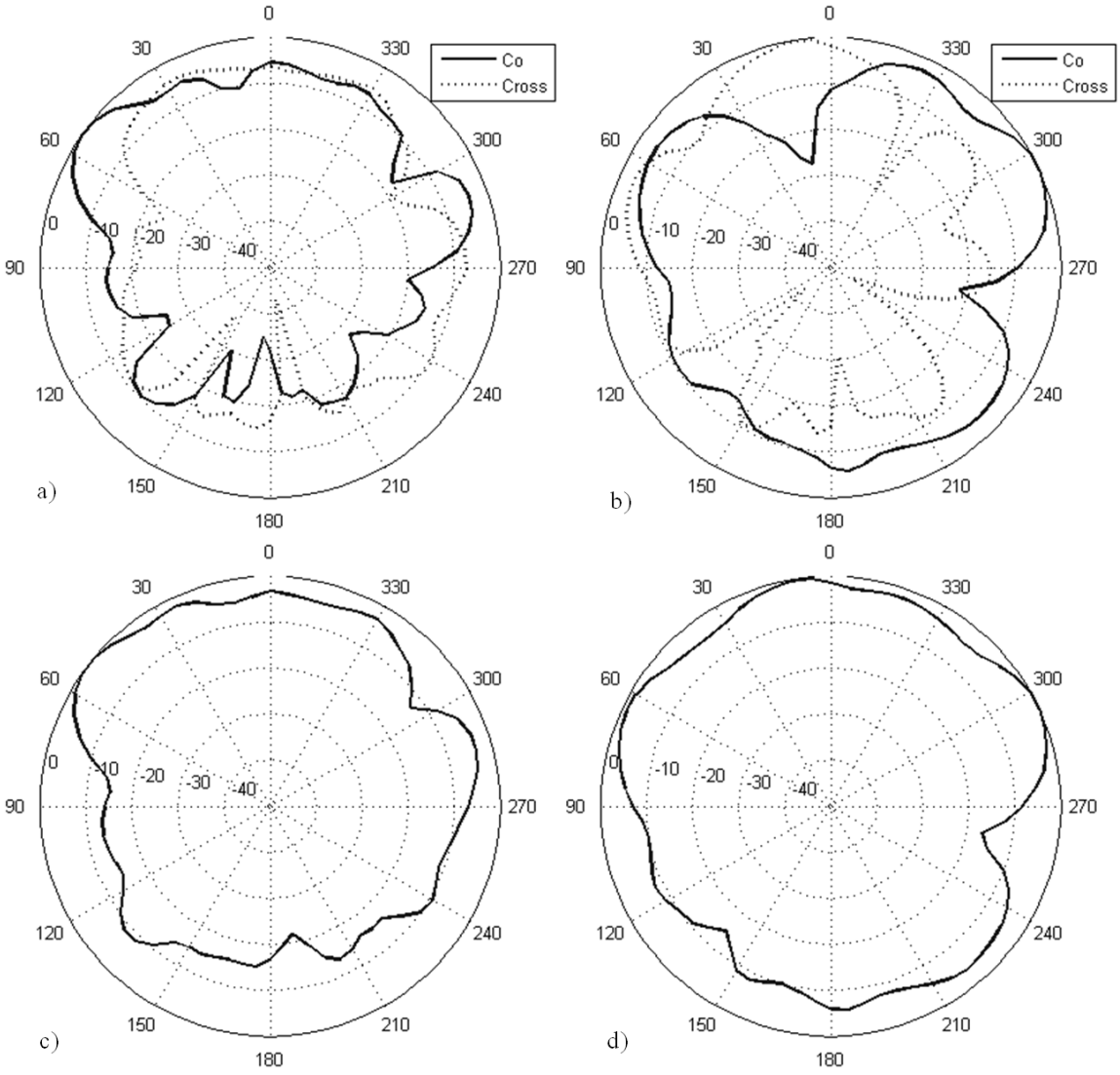

Figure 39. Radiation Patterns When Varactors are Biased at 2 V with Ground Resonance occurs at 4.02 GHz (Figure 32) a) X-Z plane b) Y-Z plane c) Total Radiation X-Z plane d) Total Radiation Y-Z plane. Refer to Figure 24 for plane reference. Patterns are normalized dB.

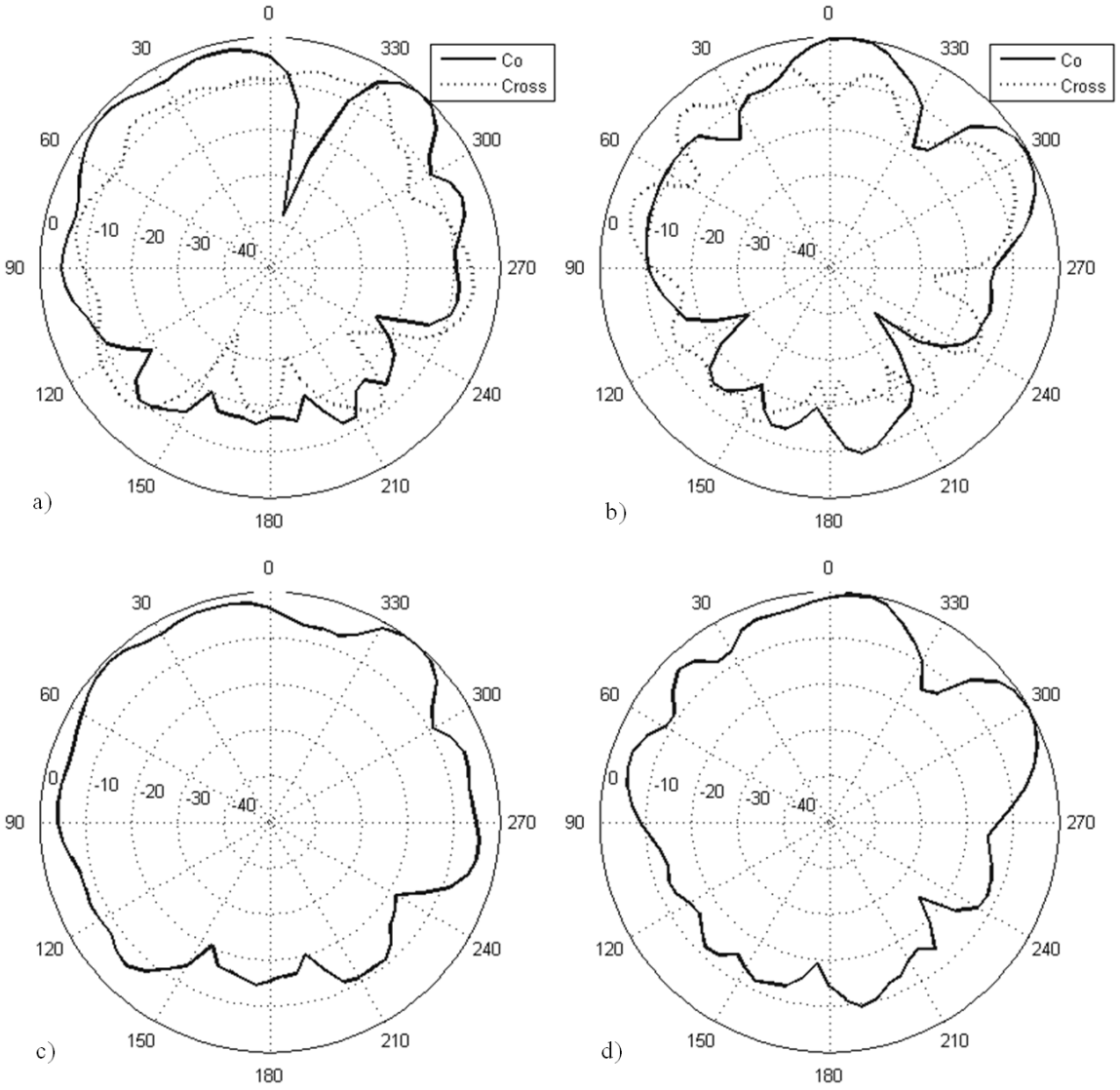

Figure 40. Radiation Patterns When Varactors are Biased at 3 V with Ground Resonance occurs at 4.17 GHz (Figure 32) a) X-Z plane b) Y-Z plane c) Total Radiation X-Z plane d) Total Radiation Y-Z plane. Refer to Figure 24 for plane reference. Patterns are normalized dB.

4.5. Discussion of Results

Figure 41 shows the simulated and experimental results for the structure at a reverse voltage of 2 V. The simulated FSS structure yields a resonance around 4.5 GHz; the simulated structure produces a resonance around 4.2 GHz; experimental results

produce a resonance around 4 GHz. Comparing Figure 29 and Figure 32 it appears the null at 3.5 GHz experimental exists at 4.5 GHz in simulations. The surface wave radiation is not present in the experimental results (6.5 GHz). The resonance at 5.25 GHz appears to be a cavity resonance because the resonance does not change frequency when the varactor is tuned (Figure 32). However, the resonance at 4.8 GHz for the simulated results appears to shift with varactor tuning (Figure 29).

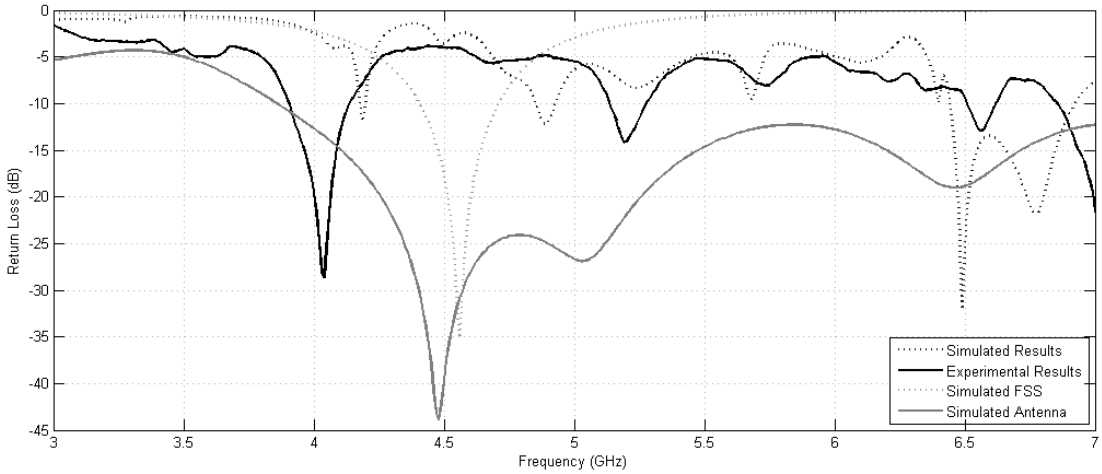

Figure 41. Measured and Simulated Results at 2 V Reverse Voltage

CHAPTER V

CONCLUSION AND SUGGESTED IMPROVEMENTS

5.1. Accomplishments

An ultra-wideband (UWB) fed tunable frequency selective surface (FSS) is proposed and investigated. The UWB antenna is an elliptical monopole antenna. The FSS is a slotted ring design with a varactor placed across the slot. The varactors are tuned through bias lines that travel through the antenna to the ground plane. The varactors provide a capacitance range (from measurement) of .24 pF (12 V) to 2.4 pF (0 V). The structure is able to tune from 3.2 GHz to 4.5 GHz. The radiation patterns show the structure no longer provides a linearly polarized wave as produced by the antenna.

5.2. Suggested Improvements

5.2.1. Beam Steering

As demonstrated in [7], an FSS, or multiple FSSs, may be used to steer an antenna beam. To produce beam steering in this application, each row of slotted rings should be biased independently to provide beam steering in one dimension. However, if each varactor is biased independently, beam steering in two dimensions can be achieved. Investigations into tuning the varactors independently and the varactors' individual effect on the resonant frequency must be performed. However, controlling the beam and resonant frequency presents an exciting achievable goal in an all-in-one package.

5.2.2. Increasing Tuning Range and Reducing Surface Wave Radiation

Though, the structure produces over 1 GHz of tuning range, investigations into increasing this range should be performed. Creating a tuning range over the entire UWB frequency could be attainable. Employing the elliptical monopole antenna with an aperture proposed in Chapter III Section 3.2.3 can produce a larger achievable range to tune. Also, the FSS structure may be modified to move the tuning range to another band.

Surface wave radiation poses a problem with spurious resonances in the UWB frequency range. Enclosing the structure in a cavity will reduce the surface wave radiation; however, this design will introduce cavity resonance modes. Investigations into this was performed, however, no suitable solution appeared.

5.2.3. Improved Radiation

The structure no longer produces linearly polarized radiation. Investigations into creating linearly polarized radiation can be performed. No emphasis was placed into polarization in this project. Investigations into placement of the varactors or adding multiple varactors may produce desirable results of polarization. Also, placing a larger ground plane will improve the back-to-front radiation of the structure.

REFERENCES

[1] Y. Lu, H. J. Lam, and J. Bornemann, "Coplanar Printed-Circuit Antenna With Band-Rejection Elements," in *Antennas and Propagation Soc. Int. Symp.* , 2008, pp. 1-4.

[2] J. Yoon, D. Kim, and C. Park, "Implementation of UWB Antenna with Bandpass Filter using Microstrip-to-CPW Transition Matching," in *Asia Pacific Microwave Conf.* , 2009, pp. 2553-2556.

[3] G. Q. Luo et al., "Filtenna Consisting of Horn Antenna and Substrate Integrated Waveguide Cavity FSS," *IEEE Trans. Antennas Propag.*, vol. 55, no. 1, pp. 92-98, January 2007.

[4] F. Bayatpur and K. Sarabandi, "Miniaturized FSS and Patch Antenna Array Coupling for Angle-Independent, High-Order Spatial Filtering," *IEEE Microw. and Wireless Compon. Lett.*, vol. 20, no. 2, pp. 79-81, February 2010.

[5] F. Bichelot, R. Loison, and L. Le Coq, "FSS-EBG Antenna with Improved Directivity Bandwidth : Theory, Design and Measurements," in *Antennas and Propag. Soc. Int. Symp.*, 2007, pp. 5423-5425.

[6] S. Zhan, R. J. Weber, and J. Song, "Effects of Frequency Selective Surface (FSS) on Enhancing the Radiation Efficiency of Metal-Surface Mounted Dipole Antenna," in *IEEE/MTT-S Int. Microw. Symp.*, 2007, pp. 1659-1662.

[7] I. Russo, L. Boccia, G. Amendola, and G. Di Massa, "Tunable Pass-Band FSS for Beam Steering Applications," in *Proc. of the 4th European Conf. on Antennas and Propag.*, 2010, pp. 1-4.

[8] F. Bayatpur, "Metamaterial-Inspired Frequency-Selective Surfaces," Electrical Engineering, University of Michigan, Ann Arbor, MI , PhD Thesis 2009.

[9] C. Mias, "Varactor-Tunable Frequency Selective Surface With Resistive-Lumped-Element Biasing Grids," *IEEE Microw. Wireless Compon. Lett.*, vol. 15, no. 9, pp. 570-572, September 2005.

[10] C. Mias, "Waveguide and Free-Space Demonstration of Tunable Frequency Selective Surface," *Electron. Lett.*, vol. 39, no. 11, pp. 850-852, May 2003.

[11] B. A. Munk, *Frequency Selective Surfaces Theory and Design*.: Wiley-Interscience, 2000.

[12] F. Bayatpur and K. Sarabandi, "Design and Analysis of a Tunable Miniaturized-Element Frequency-Selective Surface Without Bias Network," *IEEE Trans. Antennas Propag.*, vol. 58, no. 4, pp. 1214-1219, April 2010.

[13] A.C.deC. Lima and E.A. Parker, "Narrow Bandpass Single Layer Frequency Selective Surface," *Electron. Lett.*, vol. 29, no. 8, pp. 710-711, April 1993.

[14] C. Mias, "Frequency Selective Surfaces Loaded With Surface-Mount Reactive Components," *Electron. Lett.*, vol. 39, no. 9, pp. 724-726, May 2003.

[15] G. M. Coutts, R. R. Mansour, and S. K. Chaudhuri, "Microelectromechanical Systems tunable Frequency-Selective Surfaces and Electromagnetic-Bandgap Structures on Rigid-Flex Substrates," *IEEE Trans. Microw. Theory Tech.*, vol. 56, no. 7, pp. 1737-1746, July 2008.

[16] J. P. Gianvittorio, J. Zendejas, Y. Rahmat-Samii, and J. Judy, "Reconfigurable MEMS-Enabled Frequency Selective Surfaces," *Electronic Letters*, vol. 38, no. 25, pp. 1627-1628, December 2002.

[17] M. Li, B. Yu, and N. Behdad, "Liquid-Tunable Frequency Selective Surfaces," *IEEE Microw. Wireless Compon. Lett.*, vol. 20, no. 8, pp. 423-425, August 2010.

[18] A.C.deC. Lima, E.A. Parker, and R.J. Langley, "Tunable Frequency Selective Surface Using Liquid Substrates," *Electron. Lett.*, vol. 30, no. 4, pp. 281-282, February 1994.

[19] D.H. Werner and D. Lee, "Design of dual-polarised multiband frequency selective surfaces using fractal elements," *Electron. Lett.*, vol. 36, no. 6, pp. 487-488, March 2000.

[20] J. D. Kraus and R. J. Marhefka, *Antennas for All Applications*, 3rd ed. New York, NY: McGraw-Hill, 2002.

[21] Ansoft Corporation, Ansoft HFSS.

[22] F. Bayatpur and K. Sarabandi, "Single-Layer High-Order Miniaturized-Element Frequency-Selective Surfaces," *IEEE Trans. Microw. Theory Tech.*, vol. 56, no. 4, pp. 774-781, April 2008.

[23] Y. Lu, Y. Huang, Y. C. Shen, and H. T. Chattha, "A Further Study of Planar UWB Monopole Antennas," in *Antennas & Propag. Conf.*, Loughborough, UK, 2009, pp. 353-356.

[24] W. Wiesbeck, G. Adamiuk, and C. Sturm, "Basic Properties and Design Principles of UWB Antennas," *Proc. of the IEEE*, vol. 97, no. 2, pp. 372-385, February 2009.

[25] K. C. L. Chan, Y. Huang, and X. Zhu, "A Planar Elliptical Monopole Antenna for UWB Applications," in *IEEE/ACES Int. Conf. on Wireless Commun. and Appl. Comput. Electromagn.*, 2005, pp. 182-185.

[26] F. M. Tanyer-Tigrek, A. Hizal, I. E. Lager, and L. P. Lgthart, "On the Operating Principles of UWB, CPW-Fed Printed Antennas," *IEEE Antennas and Propagat. Mag.*, vol. 52, no. 3, pp. 46-50, June 2010.

[27] R. Chair, A. A. Kishk, K. F. Lee, C. E. Smith, and D. Kajfez, "Microstrip Line and CPW Fed Ultra Wideband Slot Antennas With U-Shaped Tuning Stub and Reflector," in *Progress In Electromagn. Research*, 2006, pp. 163-182.

[28] Aeroflex Metelics, "GaAs Hyperabrupt Varactor Diodes MGV Series Datasheet," Nov. 14, 2005.

[29] Skyworks, "Application Note Varactor Diodes," August 15, 2008.

[30] X. Chen et al., "Planar UWB monopole Antennas," in *Microw. Conf. Proc. Asia-Pacific Conf. Proc.*, 2005.

APPENDIX A

VARACTOR APPROXIMATION

This is the MATLAB code used to curve fit equation (1) to the varactor values given in Figure 22 given the parameters in Table 4. Figure 23 and Table 5 shows the results from the code.

```
clc;
clear all;
close all;
max = 10000000;
meas = [917 579 296 244]/1000; %average values from plot
tic;
for n = 1:max
    rd = (((rand(4,1)-.5).*.2)+1); % creates a random number vector
between .9 and 1.1 (+-10%)
    C0 = rd(1)*2.4;
    Vj = rd(2)*1.3;
    m = rd(3)*1.25;
    cp = rd(4)-.9;
    r = C0./((1.+[2 4 12 20]./Vj).^m)+cp; %equation to solve
    k = 0;
    for o = 1:length(meas)
        if(abs((r(o)-meas(o))/meas(o)) < .0065)
            % solves each point and increments if it is within .65%
error
            k = k + 1;
        end
    end
    if(k == 4)
        h2 = plot([2 4 12 20],meas,'o');
        hold on;
        x = 2:.01:20;
        fprintf('C0 = %2.4f pF (%2.2f%%)\n',C0,abs((C0-2.4)/2.4*100));
        fprintf('Vj = %2.4f V (%2.2f%%)\n',Vj,abs((Vj-1.3)/1.3*100));
        fprintf('m = %2.4f (%2.2f%%)\n',m,abs((m-1.25)/1.25*100));
        fprintf('Cp = %2.4f pF\n',cp);
        fprintf('Tries: %u\n',n);
        ylabel('Capacitance (pF)');
        xlabel('Reverse Voltage (V)');
        h1 = plot(x,C0./((1.+x./Vj).^m)+cp);
        set(h2, 'Marker', 'o', 'MarkerFaceColor', [1 1 1],
'MarkerEdgeColor', [0 0 0], 'MarkerSize', 8.0);
        set(h1, 'LineStyle', ':', 'LineWidth', 2.0, 'Color', [.1 .1
.1]);
        text('Interpreter','latex',...
```

```
        'String','$$C = \frac{C_0}{(1+\frac{V}{V_{j}})^m}+C_{p}$$',...
        'Position',[10 .8],...
        'FontSize',16)
        text(...
        'String',sprintf('C_0 = %2.4f pF\nV_j = %2.4f V\nm = %2.4f\nC_p
= %2.4f pF\n',...
        C0,Vj,m,cp),'Position',[11 .6]);
        legend('Average Measured Values of Varactors','Best Fit Curve')
        break
    end
end
toc;
if(n == max)
    fprintf('No solution found\n');
end
```